

Escarpment evolution drives the diversification of the Madagascar flora

Yi Liu^{1,2*}, Yanyan Wang^{3*}, Sean D. Willett³, Niklaus E. Zimmermann^{1,2†}, Loïc Pellissier^{1,2†}

Affiliations:

¹ Swiss Federal Research Institute (WSL); Birmensdorf, 8903, Switzerland

² Department of Environmental Systems Science, ETH Zürich; Zürich, 8092, Switzerland

³ Department of Earth Sciences, ETH Zürich; Zürich, 8092, Switzerland

*Corresponding authors. Email: yi.liu@wsl.ch & yanyan.wang@erdw.ethz.ch

#Yi Liu led the biological analyses and Yanyan Wang led the geological analyses.

Abstract: Madagascar exhibits high endemic biodiversity that has evolved with sustained and stable rates of speciation over the last several tens of millions of years. The topography of Madagascar is dominated by a mountainous continental rift escarpment, with the highest plant diversity and rarity found along the steep, eastern side of this geographic feature. Using a process-explicit model, we show that precipitation-driven erosion and landward retreat of this high-relief topography creates transient habitat organization through multiple mechanisms, including catchment expansion, isolation of highland remnants, and formation of topographic barriers. Habitat isolation and reconnection on a million-year timescale serves as an allopatric speciation pump creating the observed biodiversity.

One-Sentence Summary: Landscape and habitat transience associated with the high-relief, continental escarpment drives endemic species accumulation in Madagascar.

Main Text:

Madagascar exhibits disproportionately high biodiversity (1, 2), which has arisen in large part from its isolation from other landmasses (3). Most species in Madagascar evolved since its separation from Africa 120 million years ago (Ma) and from the Seychelles and India about 90 Ma (3, 4), resulting in extensive endemism. Although there is evidence of colonization of Madagascar by specific groups, including vertebrates (5), in the early Cenozoic, most of the subsequent speciation has been vicariant, with over 94% of mammals and reptiles and 82% of vascular plants being endemic to the island (1). However, isolation alone does not explain the high rate of *in-situ* speciation of so many taxa, and within-island geological processes and their impact on habitat distributions in space and time could help explain how this diversity has evolved (1, 2, 6).

The primary drivers of diversification in Madagascar have been suggested to be the diverse climate and changes in physical geography (6). The wet, resource-rich rainforest in eastern Madagascar is starkly different from the temperate forests, subarid, and arid bioclimatic zones of the west, and these bioclimatic zones have existed since at least the Oligocene (7), providing opportunities for adaptive speciation to the variety of habitats along this environmental gradient (8, 9). The high-relief topography of Madagascar has aided in the formation of refugia during Quaternary climate cycles (6) and provided mountain and river barriers to the dispersion of vertebrates, driving micro-endemism (10). Although these and other mechanisms for diversification have been proposed, no single process has been identified that can explain why Madagascar has such high biodiversity relative to other tropical forest regions around the world (2).

Biodiversity developed through vicariant speciation is often associated with tectonically active regions where the processes of mountain building lead to complex topography, creating new habitats, generating environmental gradients and fragmenting existing habitats (11-15). Madagascar does not fit this hypothesis well, as tectonic activity since the rifting of Gondwanaland has been minimal and localized (3, 4). However, Madagascar is surrounded by passive continental margins formed during the rifting from Africa, Australia, and, most recently, India (16), and these margins include physiographic escarpments, particularly on the east coast, which represents the youngest margin (17). The main water divide of the island marks the westward limit of the eastern escarpment, which is characterized by an increase in elevation of up to 2 km over a distance of less than 100 km (Fig. 1). The steep topographic gradient of the escarpment and the lack of a corresponding topographic gradient to the west implies a contrast in erosion rate, which drives inland retreat of the escarpment (Fig. 1, fig. S1). The escarpment appears to retreat at a nearly constant rate over the last 90 Ma has been estimated to be from 0.5 to nearly 2 km/Myr (18) (fig. S2). The escarpment retreat is superimposed on a regional geodynamic uplift that has occurred over the last 30–55 Myr, in response to deep mantle upwelling that has affected the entire island (19-21). The upwelling has maximum values in western and northern Madagascar (Fig. 1B), and it is consistent with Paleogene-Neogene marine sediments currently at an elevation of a few hundred meters (20). The island also has rift-related seismicity and volcanism, as well as surface faulting in the Alaotra-Ankay graben system, active since the Miocene (22, 23).

Landward retreat of the escarpment represents a major change to the landscape, as migration of the main water divide of the island produces a cascade of downstream dynamic changes to the topography, river network topology, and erosion rates through time (24). It is our hypothesis

that these transient and long-lived landscape perturbations result in continuously changing distributions of habitat in eastern Madagascar, providing a mechanism for allopatric or parapatric speciation. We tested this hypothesis by comparing space and time patterns of geographic and habitat change predicted by a landscape evolution model with plant phylogenies, distribution patterns and the resulting biogeographic structuring of the flora.

Timing and spatial pattern of plant diversification

We used published phylogenies to estimate the rate of accumulation of lineages and the age distribution of extant species. We generated 100 phylogenies of 8,884 Madagascar seed plants (77% of the island flora) based on a dated megaphylogeny (25) with polytomies randomly resolved. We additionally considered six time-calibrated maximum credibility trees for specific clades with species endemic to Madagascar as examples (fig. S3). The lineage through time plots, indicating the number of species that diversified from birth–death processes per clade through time, show a near-steady rate of accumulation over at least the last 45 Myr, which is supported by diversification models (Fig. 1C, tables S1 and S2). Although there is structure to the rate of accumulation, including an increase towards the present day for some clades, the timescale of accumulation is tens of millions of years and the smooth species age distribution of extant Madagascar plants reflects long, steady processes of species accumulation. In addition, there is a lack of information regarding extinction rates, due to the paucity of fossil data in Madagascar, which pulls the accumulation curve towards the present (26).

Plant species richness is highly variable across Madagascar, with the highest species richness occurring in eastern Madagascar, associated with both higher precipitation and the high relief of the eastern escarpment (Fig. 2A, B, C). Among the 8,884 seed plants mapped on the island, about 72% of the species occur along or below the escarpment of eastern Madagascar (Fig. 2A, fig S4). Orchidaceae (86%), Rubiaceae (80%), and Asteraceae (84%) are the richest families of species predominantly occurring in the escarpment area (Fig. 2D).

Transient geographic and habitat complexity

We reconstructed surface elevation change over the last 45 Myr, including mechanisms of escarpment retreat, subsidence in and around the Alaotra-Ankay graben system, dynamic uplift from mantle flow, and formation of the volcanic edifices in northern and central Madagascar (Fig. 2B, figs. S5 and S6). The reconstruction of elevation change shows that the north and west of Madagascar are dominated by dynamic uplift, punctuated by local, topographic change associated with volcanism. In contrast, eastern Madagascar is dominated by surface lowering by erosion associated with the passage of the migrating escarpment (Fig. 2B, E), with additional subsidence caused by extensional faulting.

Our results indicate a close correspondence between positive or negative changes in elevation, precipitation, and species richness (Fig. 2A, B, C). There are strong correlations between richness and escarpment retreat (fig. S7, Spearman's $r = 0.52$, $P < 0.001$) and between richness and precipitation (fig. S7, Spearman's $r = 0.66$, $P < 0.001$). Other metrics of elevation change have a weaker correlation with species richness (fig. S7). There are clear regional patterns with the highest richness corresponding to large increases or decreases in elevation in the north and east of the island, respectively (fig. S8). The orographic forcing of precipitation by the escarpment topography results in a strong correlation between escarpment retreat and precipitation rate (fig. S7), so that we cannot statistically separate the relative importance of

climate and landscape change on species richness. More importantly, statistical analyses do not capture the non-local and complex relationships where speciation is driven by time-dependent landscape change. Below, we take a different approach and attempt to characterize the land surface and habitat changes predicted by escarpment retreat in order to make more detailed predictions of the processes contributing to speciation.

To approach a causal understanding of the processes at play, we constructed a landscape evolution model simulating fluvial erosion of an escarpment on the edge of a pre-existing, topographically elevated, but weathered highland (Fig. 3, fig. S9, table S3, and movie S1) (24). The model enables documentation of the topography and habitat heterogeneity in space and time in order to assess potential mechanisms for vicariant speciation. We use the landscape evolution model *Divide and Capture* (DAC) (27), modified to predict the dynamic plant habitat as a function of surface elevation, slope and aspect. The model shows that, consistent with theory (28, 29), the escarpment retreats from the coast at a constant rate over time (24). As the escarpment retreats, drainage basins become longer and wider but growth rates are heterogeneous, and the main water divide develops sinuosity as geographically-isolated drainage basins grow at different rates (Fig. 3).

We provide a metric of landscape transience by defining habitat patches in the model as contiguous regions larger than 1 km², with elevation, slope and aspect that lie within a specified range (see methods). Through the course of the model, habitat patches are dynamic, altering their shape, size and distance from the coastline (Fig. 3, C and D). Within the escarpment region, patches frequently appear, disappear, fragment or merge (Fig. 3D, fig. S10, movies S2 and S3), promoting population isolation, allopatric speciation and micro-endemism. Splitting and merging events in the model occur at a rate of several hundred per Myr (Fig. 3D), which corresponds to an average of one event (either a split or a merge) every 2 to 5 Myr for each habitat patch (Fig. 3D, E; figs. S11 to S13), a rate consistent with speciation times in angiosperms (30). These habitat geometry dynamics are a direct consequence of the escarpment migration process; in contrast, models of mountain uplift with no escarpment or water divide migration exhibit different behavior, with an initial, short-duration transient stage, followed by almost no change in habitat pattern (figs. S11 and S14, movie S4).

The model predicts that escarpment physiographic features (Fig. 3D) disrupt north-south connectivity, fostering species turnover and local endemism. We test this prediction by coupling species range maps and phylogenies and identifying biogeographic realms characterized by marked phylogenetic turnover (Fig. 4A) along the escarpment. We clustered 10 realms by similarity and found that they are nested within three main groups differentiated by distance to the water divide and latitude with a north-south segregation (Fig. 4B, C). Geographic parameters, specifically the combination of elevation and latitude, are effective predictors (13.9% of classification error rate) of biogeographic realms, while bioclimatic parameters provide weaker associations (table S4). Latitudinal segregation of biogeographic realms also occurs between families (Fig. 4D, fig S15) and genera (figs. S16 and S17). Similar patterns have been observed in other taxonomic groups (6, 31). In addition, we computed the Margalef index as a metric of micro-endemism (32), documenting a high occurrence of rare species in the upper escarpment (Fig. 4D, fig. S18). Many species occurring in the escarpment are known only from a few localities, where 10% display extremely narrow ranges (distances between occurrences of < 25 km; fig. S19). Biogeographic segregation along the escarpment, a high rate of occurrence of rare species, and a high frequency of restricted distribution (fig. S20) are characteristics that support the thesis that habitat fragmentation along the escarpment controls speciation.

Changes in topography associated with escarpment retreat may impact speciation rates through a number of potential mechanisms. First, the westward migration of the escarpment and its orographic influence on precipitation (Fig. 2, fig. S1C) implies an expansion of the tropical forest habitats with their greater productivity, and opportunities for ecological specialization (12, 14). Second, escarpment migration implies movement of the main water divide through drainage area capture, a discrete, episodic process whereby individual river basins advance their headwater reaches into the highlands (Fig. 3A). The episodic nature of this process implies downstream variations in erosion rate and surface morphology in space and time, leading to temporally variable habitat and the strength of river barriers. Third, differential retreat rates imply that some catchments become isolated from the main divide (e.g. basin (b) in Fig. 3A, B). Many of these geographic features have been demonstrated to be important in driving speciation (2). For example, isolated catchments have served as centers for endemism (6), and large rivers have acted as barriers to Lemur dispersion (10). Although most past studies have focused on animals and it is difficult to associate specific speciation events with specific processes, the close correlation of species richness and rarity with the active escarpment provides circumstantial evidence that some combination of these processes have been responsible for an increased speciation rate across multiple taxa.

Differentiating climate from geomorphic process

The escarpment and topographic highlands have a strong orographic effect on the precipitation pattern across Madagascar such that the bioclimatic zone and the escarpment geomorphic domain correspond almost perfectly, and both correlate with the region of high species richness, making it difficult to distinguish between high speciation rate and a high, climate-modulated species carrying capacity. Tropical moist forests, as in eastern Madagascar, are associated with a higher biomass, capable of sustaining higher levels of diversity through larger populations and unique niche formation (33), and the tropical forest area increases in size as the escarpment moves west. Adaptation along the west–east climate gradient offers opportunity for dry-climate species to adapt to the wetter environments, or vice versa. Climate change associated with moist–dry cycles during the Quaternary may also have impacted speciation rate through habitat fragmentation and reconnection (34). However, there are three lines of evidence that support geomorphic-driven vicariance. First, the phylogenetic analysis (Fig. 1C, table S2) shows a near constant rate of diversification over at least the late Neogene, with no acceleration during the Quaternary when climate cycles became more pronounced (35). Second, the latitudinal turnover and species rarity distribution (Fig. 4D, fig. S18) have no direct climatic association, given the lack of North-South climate variability. In contrast, the landscape evolution model predicts transient changes in habitat connectivity in the north-south direction, associated with changes in the large rivers and interfluvial ridges, consistent with the species turnover pattern. Third, the timescale of habitat fragmentation by climate change is much faster than we predict for geomorphic transience. Quaternary climate cycles have periods from 22 to 100, 000 years (35), whereas geomorphic transience in Madagascar creates habitat patches with a typical isolation time of several millions of years (Fig. 3D, E), more consistent with the empirical observations for speciation time in plants (30).

Implications for the importance of geomorphic vicariant speciation

Madagascar can serve as an example of how speciation is enhanced by comparably small-scale geomorphic landscape dynamics, driving micro-endemism. While the importance of catchment geography for Madagascar’s micro-endemism has been recognized (2), our analyses suggest

that catchment geometry and other geomorphic characteristics are highly transient in response to escarpment migration. Lateral migration of an escarpment or a water divide is more disruptive to a landscape than vertical tectonic uplift, because disruption of the planform geometry of a river network triggers a downstream chain of perturbation, creating yet more heterogeneity in physiography and longer response times (compare Fig. 3 with fig. S11) (36). These perturbations result in lower habitat connectivity (37), fragmentation and reconnection (fig. S11). This process is evident in the segregation of lineages and the spatial pattern of diversity and endemism. Although we focused on plant habitat parameters in our model, the limited range sizes and latitudinal segregation are representative of other taxa in Madagascar, including lemurs (6) and amphibians and reptiles (31), which show distributions closely matching features of the escarpments.

There are other settings around the world where geomorphic disequilibrium and high biodiversity co-exist. The Western Ghats of India on the conjugate margin to Madagascar also display a high level of plant endemism (38). The rift margins of Brazil, South Africa, and parts of Australia similarly stand out as regions with transient escarpments and high endemism (30, 39). Likewise, southeastern North America retains a high degree of geomorphic disequilibrium and aquatic species diversity 180 million years after its formation as a continental margin (40, 41). High biodiversity observed in other tectonic settings characterized by geomorphic transience and habitat fragmentation include the East African rift (42) and the Andean foreland (43). Our results suggest that the complex dynamic response of the landscape to tectonic forcing can persist for tens or even hundreds of millions of years and that the consequent disequilibrium leads to shifting patterns of habitat connectivity in both space and time, acting as a speciation pump to increase biodiversity long after the cessation of tectonic activity.

Acknowledgments: We thank the reviewers who provided constructive comments that improved the manuscript. **Funding:** Y.L. thanks the Chinese Scholarship Council (CSC) (201904910589) and WSL for its financial support. Support was received from the ETH Research Commission through the BECCY project. **Author contributions:** Conceptualization: Y.L., Y.Y.W, S.D.W, N.E.Z, L.P.; Methodology: Y.L., Y.Y.W., S.D.W., N.E.Z., L.P.; Investigation: Y.L., Y.Y.W., S.D.W., N.E.Z., L.P.; Visualization: Y.L., Y.Y.W.; Funding acquisition: Y.L., S.D.W., N.E.Z., L.P.; Project administration: Y.L., N.E.Z., L.P.; Supervision: S.D.W., N.E.Z., L.P.; Writing: Y.L., Y.Y.W., S.D.W., N.E.Z., L.P. **Competing interests:** The authors declare that they have no competing interests. **Data and materials availability:** The landscape evolution model used in this study, DAC (56), and codes for the habitat patch change analysis of the landscape evolution models (57), are available at Zenodo repositories. The data generated, analyzed, and presented in this study is available from the EnviDat repository (58).

Supplementary Materials

Materials and Methods

Figs. S1 to S20

Tables S1 to S7

References

Movies S1 to S4

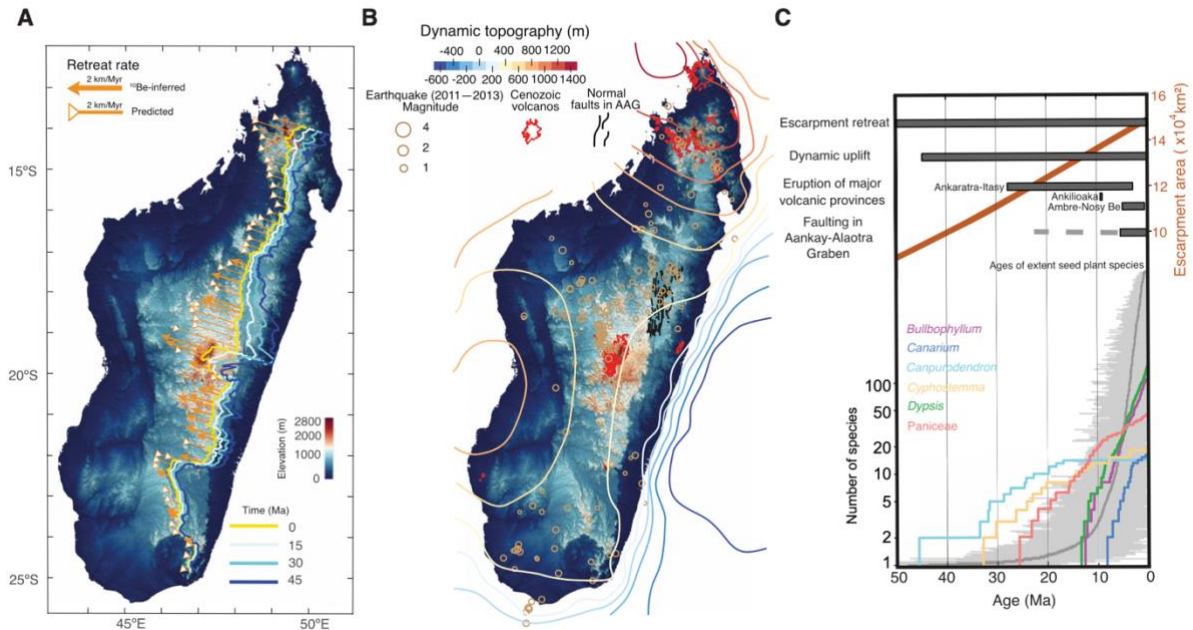


Fig. 1. Surface uplift, erosion, and plant lineage accumulation in Madagascar. (A) Escarpment position estimates over the past 45 million years (Myr) based on modern retreat rates (arrows). Escarpment retreat has resulted in nearly 2 km of erosion and surface lowering. (B) Spatial distribution of additional surface uplift processes, including dynamic uplift from mantle flow (contours of cumulative uplift), active surface faulting (black lines), and volcano formation (red polygons). Seismicity is indicated by yellow circles. (C) The upper panel illustrates the estimated timeframe of landscape change [solid bars indicating age constrained by geological evidence (4, 18 – 23, 44 – 48) and the dash line indicating poorly constrained age]. Orange line indicates average change of area below the escarpment. The lower panel displays the accumulation of plant lineages over time. The mean ages of 8,884 extant seed plant species, estimated from 100 reconstructed phylogenetic trees, are indicated by the dark grey curve. The horizontal light grey lines represent the standard deviation around the mean of individual species ages. The colored lines represent the lineage through time plots of six example clades from dated phylogenies (49 - 54).

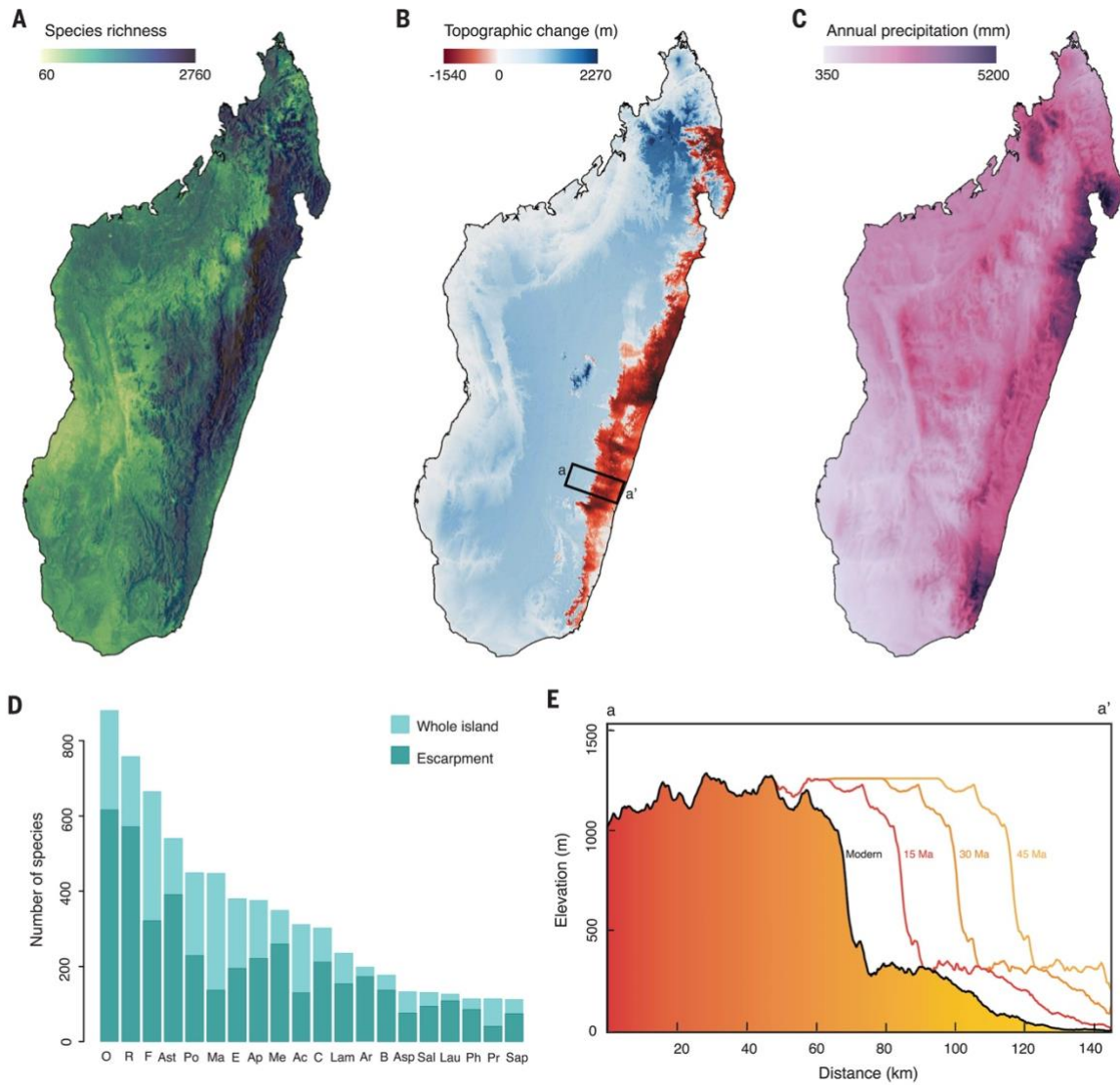


Fig. 2. Biodiversity of seed plants, topographic change and mean annual precipitation in Madagascar. (A) Species richness map of 8,884 seed plants on the contemporary Madagascar landscape. (B) Estimate of topographic change over the last 45 Ma based on combined effects of the four processes listed in Fig. 1C. (C) Map of contemporary annual precipitation in Madagascar [available at <http://chelsa-climate.org> , (55)]. (D) Total number of species occurring on Madagascar (turquoise) and distributed along the escarpment (dark turquoise) in the top 20 species-rich families : Ac, Acanthaceae; Ap, Apocynaceae; Ar, Arecaceae; Asp, Asphodelaceae; Ast, Asteraceae; B, Balsaminaceae; C, Cyperaceae; E, Euphorbiaceae; F, Fabaceae; Lam, Lamiaceae; Lau, Lauraceae; Ma, Malvaceae; Me, Melastomataceae; Ol, Oleaceae; Or, Orchidaceae; Ph, Phyllanthaceae; Po, Poaceae; R, Rubiaceae; Sal, Salicaceae; Sap, Sapindaceae. (E) Topographic reconstruction of escarpment retreat of the selected region (a-a', window size: 50 × 145 km) over the last 45 Ma.

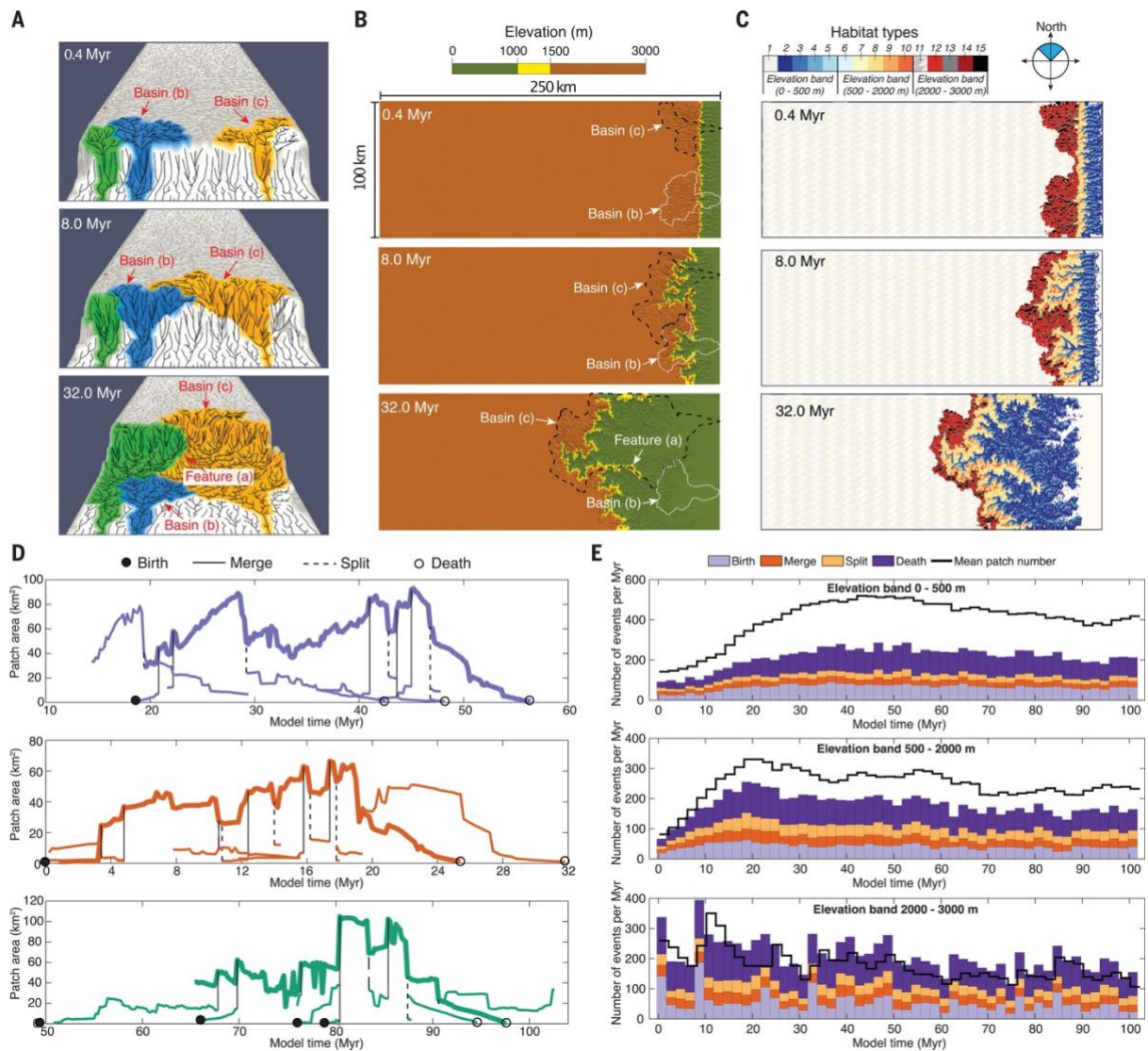


Fig. 3. Landscape evolution model simulating retreat of a segment of the Madagascar escarpment. (A) Perspective view of the escarpment with three drainage basins highlighted. Main water divide migrates inland at a rate of 2 km/Myr, expanding the area of the coastal plain. (B) Topographic isolines during escarpment retreat. (C) Nominal plant habitat distributions defined from elevation, slope and aspect of the landscape (table S5). (D) Examples of the area evolution of habitat patch groups within the model; the bold line indicates a focus patch, and the fine lines showing neighbor patches that merge or split with a focus example. Birth, death and area changes are also indicated. (E) Number of habitat patches (black line), as defined in Fig. 3C, and the rate of birth, death, split and merge (events per Myr), grouped into three elevation ranges. Feature (a) indicates isolated highland remnants. Basin (b) indicates a catchment that initially drained from highland elevations but is subsequently confined to lowland regions. Basin (c) is an expanding basin, increasing in drainage area.

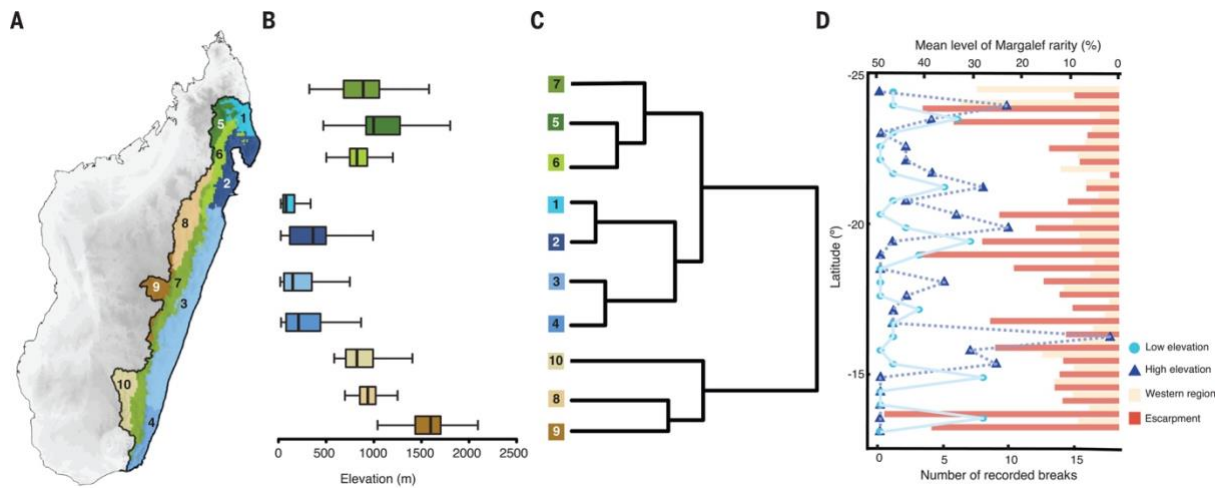


Fig. 4. The biogeographic realms of seed plants in eastern Madagascar. (A) Realms are defined by phylogenetic turnover ($p\text{-}\beta\text{sim}$) in range maps. (B) Elevational range of each biogeographic realm. (C) Dendrogram representing the similarities in the composition of plant lineages between the 10 distinct biogeographic realms. (D) Density of breaks separating different biogeographic realms along the escarpment based on the biogeographic realms of the top 20 species-rich families in low-elevation (coastal) and high-elevation areas. To compare the Margalef rarity along the escarpment and the western region at the same latitude, we estimated the rarity on a 50-km-resolution grid and subsequently averaged within each interval.

Supplementary Materials for
Escarpment evolution drives the diversification of the Madagascar flora

Yi Liu *et al.*

Corresponding authors: yi.liu@wsl.ch & yanyan.wang@erdw.ethz.ch

The PDF file includes:

Materials and Methods
Figs. S1 to S20
Tables S1 to S7
Movies S1 to S4
References

Other Supplementary Materials for this manuscript include the following:

MDAR Reproducibility Checklist
Movies S1 to S4

Materials and Methods

Topographic change model

Escarpment retreat

The Madagascar escarpment follows the major divide of the island for 1200 km from south to north (Fig. S1A). The modern escarpment is ~30–110 km inland of the eastern coastline. The topography across the water divide is asymmetrical in that the east-facing escarpment is steep and bounds the relatively low-relief high plateau (Fig. S1D). The erosion rate of the escarpment is higher than that on the plateau (Fig. S1B), a process enhanced by the precipitation gradient (Fig. S1C) (59). The Köppen-Geiger climate classification of Madagascar shows a decrease in precipitation and an increase in temperature seasonality from the coast to the plateau (60). Given the asymmetrical topography and the differential erosion rates across the divide, the escarpment front retreats towards the west. The continuous retreat of the escarpment enlarges the coastal plain area, shrinks the plateau area, and maintains the asymmetrical topography across the divide, in a process active since the Cretaceous rift with Seychelles-India (18). We quantified the topographic change of escarpment retreat using a back-stripping method. We assumed that the plateau elevation, the retreat rate, and the retreat direction of the escarpment remained constant temporally. We set retreat direction at N73W, orthogonal to the east coastline. We reconstructed the position of the plateau–escarpment boundary by translating the topography eastward, at the rate of retreat, v (Fig. 2E). The topographic change was the elevational difference between the reconstructed topography and the modern topography. We measured the retreat rate, v , over most of the southern segment (18), using cosmogenic nuclide isotope concentrations of ^{10}Be (Fig. S2A, B). For basins with no cosmogenic isotope data, we estimated the retreat rate through linear interpolation of the two bounding retreat rates (Fig. S2C). In the northern segment, we used a scaling relationship between the retreat rate and the plateau height to estimate the retreat rate from the plateau height (Fig. S2B, C).

Mantle dynamic uplift

We used the dynamic topography from the global dynamic topography model of Davies et al. (61), which includes a correction for the shallow mantle and lithospheric structures. The original raster data had a resolution of 0.1° . We extrapolated data to the 1 km grid for Madagascar using linear interpolation. The dynamic uplift of Madagascar probably started in the mid to late Cenozoic, although it is possible that it started somewhat earlier, following the rift between Madagascar and Seychelles-India in the late Cretaceous, around 120–84 Ma (4, 44, 45). Cenozoic dynamic uplift of Madagascar is supported by the occurrence of Oligocene-Pleistocene volcanism (46), uplift and exposure of Eocene-Miocene carbonate platforms on the western coastal plain, and sedimentary units containing marine fossils (20). In this study, we assumed that the observed dynamic topography has increased since 45 Ma, which corresponds to the oldest Cenozoic marine fossils that are exposed at the northern tip of the island (47). The dynamic uplift rate of Madagascar is in the range of 5–30 m/Myr, assuming an onset date of 45 Ma. Except for the higher rates in the far north, Madagascar has had a relatively moderate uplift rate of 10–15 m/Myr. The higher dynamic uplift rate, which is in the range of 25–32 m/Myr in northern Madagascar, could be overestimated in the dynamic uplift model because of the pronounced topography that was built by the extensive Pliocene-Pleistocene volcanoes in this area. The surface elevation change from mantle dynamic uplift is reduced by accompanying erosion and the fact that the initial topography was sometimes

below sea level especially at the western margin of Madagascar. Erosion or an initial water depth act to reduce the surface uplift due to mantle flow. Surface erosion outside the escarpment region is limited (62), but could be significant in coastal regions. We apply both erosion and initial water depth as a limit, truncating the mantle uplift if it predicts topography higher than the modern. Surface elevation change due to mantle dynamic uplift is provided as the minimum between modern topographic elevation and the dynamic topography predicted by Davies et al (61). Volcanic edifices were removed from the modern topographic elevation before this calculation.

Faulting in the Ankay-Alaotra graben system

The Ankay-Alaotra graben system is formed from a series of north–south oriented normal faults (22, Fig. S5A, B). Faulting activity in the graben are heterogeneous in space, showing three sub-domains (22, 48). The southern sub-domain, the Ankay graben, shows asymmetrical faulting in that the eastern horst is substantially lower than the western horst, whereas the northern sub-domain, the Alaotra graben, is a full graben showing symmetric horst–graben–horst topography (Fig. S5C, E). The sub-domain in the middle is the Andaingo Heights, which has a symmetric full-graben form but limited fault throw (Fig. S5D). For each sub-domain, the western horst actively functions as the island’s water divide, separating the high plateau to the west from the escarpment to the east (Fig. S5B). The timing of initiation of the graben faulting is poorly constrained. It could be related to volcanism of the Ankaratra volcanic massif in the early Neogene (46), as both indicate a large-scale extensional environment of the crust. Post-Miocene activation of faulting of the graben is supported by uplifted Pliocene sediment, Pliocene intrusion of plutonic rocks, and active quaternary subsidence of the graben floor (23). Nevertheless, the activation of the graben is broadly within the period of 45 Ma to modern time. Lowering of the graben surface relative to the horst creates accommodation space for sediment to be deposited in the graben. Sedimentation on the graben floor causes secondary isostatic subsidence. Sediment thickness in the Ankay-Alaotra graben varies from a few tens of meters to 200–300 m (23). In this study, we defined the modern land surface as the resultant surface deformed from multiple faulting-related processes, including sedimentation. We used the island divide coinciding with the western horst of the graben as the reference surface level. The graben surface is relatively low, and we took the elevation difference between the divide and the graben floor at the top of the sediments to be the topographic change due to faulting (Fig. S5C). We defined the topographic change of a location in the graben as the elevation difference between this location and the elevation of its reference divide, where the reference divide is the projection of the interest location in the direction of N73W (Fig. S5C).

Construction of volcanic edifices

Cenozoic volcanic activity in Madagascar is clustered into three regions, the Ankaratra-Itasy volcanic province on the central plateau, the Ambre-Nosy Be province in the north, and the Ankililoaka in the southwest coastal plain (46). The volcanic eruption age of provinces varies from Late Oligocene to Pleistocene (46), falling in the period of interest of 45 Ma to the present. Eruption of volcanoes can directly build up topography, forming volcanic mountain peaks, or change the topography by overland lava flows. To calculate the topographic change due to volcanic activity, we assumed that the marginal area surrounding the volcanic area is unaffected. We used the mean elevation of the marginal rim as the reference elevation for each mapped volcanic patch (Fig. S6). We took the elevation difference between the volcanic area and its surrounding marginal rim to be the topographic change due to volcanic eruption (Fig. S6). We used the geological map by Roig et al. (63) to extract the Cenozoic volcanic patches.

Analyzing the diversification of Madagascar clades

To investigate the species accumulation through time, we considered species-level phylogenies. We used previously published maximum clade credibility (MCC) trees with calibration information from six clades [Paniceae from (49), *Bullbophyllum* from (50), *Canarium* from (51), *Capurodendron* from (52), *Cyphostemma* from (53), and *Dypsis* from (54)], and we generated the lineages-through-time (LTT) plots. To test the steady rate of accumulation of lineages through time, we fitted six diversification models to each of the six phylogenies using maximum likelihood (64). We examined two types of models, with diversification rates that were constant (2 models) or time-dependent (4 models), as described in Table S1. We modeled diversification as a two-rate process, where $\lambda_0(\mu_0)$ corresponded to the rate of speciation (extinction) of the clade. The constant diversification consisted of a pure-birth model (no extinction, $\mu_0 = 0$) and a model with fixed rates of speciation and extinction. In the time-dependent models, $\lambda(t) = \lambda_0 e^{\alpha t}$ and $\mu(t) = \mu_0 e^{\beta t}$, we assumed that speciation and (or) extinction events follow a Poisson process characterized as a continuous function of time, where the parameter α (β) quantifies both the direction and the magnitude of temporal dependence. We implemented these models with maximum likelihood using the ‘fit_bd’ function from the *RPANDA* 1.9 (65). We identified the best-fitting model using the lowest AICc score (66). In addition, we used a time-calibrated species-level plant megaphylogeny, GBOTB, that was incorporated into the *V.Phylomaker* 0.1.0 (67) as a backbone tree for constructing phylogenies of Madagascar seed plants. Smith and Brown (25) built the original phylogenetic tree using molecular data of 79,881 taxa in GenBank and dated it according to Open Tree of Life, version 9.1 (ALLOTB). Currently, it is considered the largest dated megaphylogeny for seed plants. We checked for concordance between the names at the tips of the phylogenetic tree and the species in our checklist. Together, this resulted in a list of 8,884 seed plants in 215 families and 1,453 genera. To estimate species ages, we generated 100 phylogenies using the ‘phylo.maker’ function under *scenario 2* in *V.Phylomaker* 0.1.0 (67). Specifically, missing species from the backbone tree were incorporated as the new tips and bound to randomly between dated nodes and terminals within their genus or family. To account for uncertainty, we calculated the mean and standard deviation of species ages based on the 100 repetitions.

Species range mapping

We used a combination of species distribution models (SDMs) (68) and geographic range polygons to estimate the geographic distribution of individual species from occurrence data. We compiled a checklist of seed plant species from *Catalogue of Vascular Plants of Madagascar* (69) (<http://www.tropicos.org/Project/Madagascar>), which includes descriptions of species distributions in terms of administrative regions, elevation ranges and habitat types. In addition, we obtained records of localities of species from several sources: Global Biodiversity Information Facility (70) (GBIF, <https://www.gbif.org>), Botanical Information and Ecology Network (71) (BIEN, <https://bien.nceas.ucsb.edu/bien/>), Integrated Digitized Biocollections (72) (iDigBio, <https://www.idigbio.org/>), and RAINBIO (73) (<https://gdauby.github.io/rainbio/index.html>). We standardized species scientific names using the GBIF Backbone Taxonomy, accessed through the R package *rgbif* 3.6.0 (74). We merged the infraspecific taxa at the species level. After cleaning (75), we kept 8,884 species and 254,079 occurrence records. We extracted the environmental variables that we used for SDMs from Climatologies at High resolution for the Earth Land Surface Area (CHELSA version 2.1) (55) and SoilGrids (76). All predictors were kept at or aggregated to 1 km × 1 km resolution and projected to the WGS 84/UTM zone 38S (EPSG: 32738). To avoid collinearity among the variables, we conducted a correlation analysis and selected five predictors

where the inter-correlation was less than the absolute value of 0.7, namely: (i) mean temperature, (ii) annual precipitation, (iii) precipitation seasonality, (iv) volumetric fraction of coarse fragments (> 2 mm), and (v) proportion of silt particles (≥ 0.002 mm and ≤ 0.05 mm) in the fine-earth fraction. According to the number of occurrences of the species, we performed two procedures in our SDMs. For species with 20 or more unique occurrence points, we followed the approach of Lyu et al. (77) to build SDMs that fitted generalized linear models (GLMs) (78), generalized additive models (GAMs) (79), gradient boosting machines (GBMs) (80), and random forests (RFs) (81) with three different levels of complexity (82). We randomly sampled pseudo-absence points, with a maximum of 50,000 points, and we tested the models using three-fold cross-validation. We summed the predicted presence of six models with the highest scores in true skill statistic (TSS) (83) and kept the overlap area as the species geographic range. In the case of species with fewer than 20 unique occurrence points, we first compiled species information regarding their geographic distribution within administrative regions, elevational information, and habitat type information, following their descriptions in the checklist. We then mapped their distribution using raster files of elevational bands using a digital elevation model (84) (<https://srtm.csi.cgiar.org/>) and habitat type information from the *Madagascar Vegetation Map* (85), where we classified species' habitat types to match the vegetation. We generated distribution polygons of these species by clipping administrative boundaries, elevation ranges and habitat preference maps. We then built SDMs and constructed ensemble distribution maps in a similar way as for those with more than 20 occurrence points. For each species, we randomly sampled a maximum of 7,500 pseudo-absence points and fitted the models using the intermediate level of GLM, GAM and GBM. We constructed convex-hull polygons for each species' geographic boundary based on occurrence and administrative boundary data. From the habitat information, we assigned ecoregions (86) in which the species can occur. We then created an overlap of bioregion and convex hull to exclude SDM predictions in areas outside this overlap polygon. We built various buffer distances (ranging from 90 km to 370 km) around the bioregions based on the distances between species occurrences to simplify the shapes of the species range polygons. Finally, we derived species richness and weighted endemism maps by overlaying individual species distribution maps. We compared the levels of endemic richness in and out of the escarpment with a variant of Laffan and Crisp's weighted endemism metric (87):

$$WE = \sum_{t \in R} \frac{r_t}{R_T}$$

where R_T represents the complete geographic range of taxon t , while r_t denotes the local range of taxon t . We quantified both values based on the number of grid cells using species distribution maps.

We assessed the association between species richness, precipitation and four geological processes affecting topography (escarpment retreat, mantle-driven uplift, volcanism, and active fault tectonics) using Spearman's rank correlation coefficients. We used a two-sided hypothesis test to determine the statistical significance of correlations based on Spearman's rho statistic. To illustrate the spatial association between environment and richness across different areas of Madagascar, we conducted a principal component analysis (PCA) using the function *dudi.pca* from the package *ade4 1.7-17* (88) including elevation change values of each afore mentioned process together with precipitation. To visualize their geographic patterns, we delineated three distinct areas: the escarpment, the western region, and the north of the island. The boundary between the escarpment

and the western area is determined by the primary water divide of the island. The northern limit represents the border of the area experiencing the strongest uplift (16 °S). We further related species richness to elevation change from the different processes and precipitation with a generalized linear model (GLM) and computed the explained deviance of the model.

Landscape evolution model

In the landscape evolution model *Divide and Capture* (DAC, 27), the topography is explicitly described by an irregular numerical grid with nodes representing rivers. Diffusive hillslopes and water divides are sub-grid features whose location and height are analytically determined from the incision rate of the rivers (27). DAC features dynamic river network reorganization through captures and divide migration (27), both of which are important in characterizing a landscape and the topographic evolution. River incision in DAC is governed by the stream-power incision law, where the incision rate scales with drainage area, precipitation, rate, river slope, and an empirical parameter, which is usually referred to as erodibility to characterize the erosion resistance of the substrate (89).

In this study, we conducted the landscape evolution model of the escarpment using the initial escarpment topography and river network (Fig. S9A). The rivers incised into the pre-existing plateau, where a thin layer of heavily weathered, more erodible rock mantles the plateau, covering the underlying erosion-resistant crystalline bedrock (Fig. S9B) (24). The weathered layer was represented by the layer thickness, Thw , and the erodibility, Kw . The erodibility of the fresh crystalline bedrock was given by Kb . The weathered layer on the plateau was progressively eroded once it was captured by escarpment rivers (Fig. S9, Movie S1). Parameter values used in the model are given in Table S3.

To provide contrast for the landscape characteristics of the escarpment model, we constructed a model with a spatially constant uplift rate, resulting in topography with a stable configuration of rivers and water divides. At steady state, the mountain range was symmetric with the major water divide in the middle of the domain. At equilibrium, the topography had a steady height similar to the plateau in the escarpment model (Fig. S14A, Movie S4). Parameter values used in this model are given in Table S3.

Habitat analysis of the landscape evolution models

To quantify the landscape change and impact on habitat, we defined habitat in terms of the hillslope aspect, the hillslope gradient, and elevation of the land surface of the numerical landscape evolution models. These three physiographic landscape metrics are commonly used to characterize habitats (90, 91). We defined fifteen combinations of value ranges of these three metrics for the numerical land surfaces (Table S5).

There are other parameters that are important to plant habitat, including a range of climate parameters and soil characteristics. In Madagascar, precipitation is very important at the scale of the island, but at the scale of the escarpment it is relatively constant (Fig. 1) and therefore would not greatly influence the habitat as we have defined it. However, we acknowledge that there are likely smaller-scale orographic forcing effects and micro-climate zones that are not apparent at the scale shown. Soil properties could also be important determinants of habitat, in particular given the prevalence of nutrient-poor laterites on the central plateau of Madagascar. Erosion of the

escarpment could have an independent effect on diversity through the release of mineral nutrients, but we did not investigate this aspect of the problem.

Habitat patch change in space and time

Our landscape evolution model used an irregular grid. To perform the habitat patch analysis, we interpolated the land surface (x, y, z) to a regular mesh. The land surface was represented by a set of elemental surfaces. We calculated the elevation, slope gradient, and slope aspect for each elemental surface, and we assigned the habitat type according to Table S5. We defined a habitat patch as a contiguous area that consists of elemental surfaces of the same habitat type. We analyzed habitat patches that were larger than a critical area of 1 km², which is about 100 grid cells in the regular mesh. We tracked the temporal and spatial change in habitat patches for each habitat type.

The patch size and shape evolved dynamically during the landscape evolution (Movies S2, S3). Numerically, we used unique indices to label habitat patches. We used patch size (area) and intersections of habitat extent between patches in consecutive steps to characterize different types of patch changes (Fig. S10). For convenience, we will use the terms ‘previous step’ and ‘current step’ to describe an example of two consecutive steps. We identified five types of patch change, and we counted the number of events of each type for both the escarpment retreat model and a block uplift model (Fig. 3E, Fig. S10).

1. Death. A pure death event is defined as an event in which a patch exists in the previous step but disappears in the current step. The “disappearance” is defined numerically when the patch area falls below the critical area.
2. Birth: A pure birth event is defined as an event in which a patch does not exist in the previous step but appears in the current step. The “appearance” is defined numerically when the patch area is greater than the critical area.
3. Split: A situation where a single patch in the previous step has two or more patches that intersect with it in the current step. Pure birth and birth from split are distinguished in our model.
4. Merge: A situation where two or more patches in the previous step intersect with a single patch in the current step.
5. Deform and migrate: A situation where a single patch in the previous step intersects with one patch in the current step. The patch size and shape differ between the two steps.

Characteristic timescales

Timescales of habitat patches and their changes scale with the landscape evolution rate, which we characterized in this model by the retreat rate for the escarpment. We quantified the number of births, deaths, splits and merges within the model over a unit of time. Space normalization could be done by area, but we preferred to normalize by the total number of habitat patches, so that the frequency was expressed in terms of a probability of change for an individual patch.

The critical timescale for vicariance is the time during which a population or habitat patch remains isolated from other patches. A patch could appear by birth and disappear by death, but this was rare (Movie S3). More often, a patch had a complicated history of area change through split and merge events (Fig. 3D). Here, we present the average time that a patch was likely to be unaffected by merge and split events, which we defined as the recurrence time of merge or split events of a habitat patch. The recurrence time for a patch split on the escarpment was 4–10 Myr, and the recurrence time for a merge was similar (Fig. S11B, C). Recurrence time was longer for habitat

patches in the low-elevation region (Fig. S11A). This frequency scaled linearly with the escarpment retreat rate. In the model shown, the escarpment retreat rate is 2 km/Myr, which is at the upper limit of the estimate for Madagascar.

Landscape evolution and habitat sensitivity analysis

To contrast the retreating escarpment model with other tectonic settings, we ran the habitat analysis on a model of an uplifting block with no escarpment and minimal divide motion. In the block uplift model, the landscape shows transience in the initial stage of the model as a plateau is uplifted and eroded at its margins (Fig. S14A, Movie S4). New habitat patches are formed and there are frequent habitat patch changes in the landscape transient stage (Fig. S14B). At steady state, the landscape is static, whereby the major ridges, valleys and major divide remain steady in space and height (Movie S4). The patches also remain static so that the patch number stays constant and few patch changes happen (Fig. S14C). The recurrence time of split and merge events is a few hundreds of million years to infinite at the landscape steady state (Fig. S11D to F).

We analyzed the robustness of the type and frequency of habitat patch changes by conducting a similar patch analysis using different parameters for the habitat types, but keeping the landscape evolution model the same. We describe the parameters as habitat model 2 (Table S6). Habitat model 2 used five elevation bands and aspect and hillslope gradient ranges, as in habitat model 1. The frequency and types of patch changes were also similar to those in habitat model 1 (Fig. S12). The larger number of habitats in habitat model 2 resulted in a larger number of habitat patches, but the frequency or recurrence times of splits and merges remained almost the same. (compare Fig. S13B, C with Fig. S11B, C).

Phylogenetic regionalization

As a means of understanding the spatial and evolutionary patterns of biodiversity, we applied a phylogenetic regionalization approach to delimit biogeographic units. We conducted cluster analysis of assemblages of species based on pairwise matrices of phylogenetic beta diversity. We calculated phylogenetic beta diversity using the Simpson index of dissimilarity (hereafter “p- β sim”) (92, 93), which is not sensitive to differences in species richness among compared assemblages. It can provide an unbiased estimation of compositional turnover among grid cells and is calculated as:

$$\beta sim = 1 - \frac{a}{\min(b, c) + a}$$

where a is the number of shared species between two grid cells and b and c represent the number of unique species in each grid cell, p- β sim measures the dissimilarity with the minimum difference between b and c . Based on the equation used for β -sim, we calculated p- β sim measures using shared and unique branches rather than species (94, 95). For the computation, we first aggregated the species distribution maps to a 5 km \times 5 km resolution and clipped their range maps to the escarpment region, then combined the maps with a global phylogeny (Fig. S4) generated by *V.Phylomaker 0.1.0* (67) under *scenario 3*. In order to select the best-fitting clustering algorithm, we tested the performance of eight algorithms (96) (single linkage, complete linkage, unweighted pair group method with arithmetic mean (UPGMA), unweighted pair group method using centroids (UPGMC), weighted pair group method with arithmetic mean (WPGMA), weighted pair group method using centroids (WPGMC), and Ward’s minimum variance criterion (Ward’s D) and its modification (Ward’s D2)) with the global phylogeny. Considering both efficiency and

accuracy (Table S3), we selected UPGMA for the final analysis. For efficiency, we compared the explained variance of the data set with the optimal number of clusters in every algorithm. However, the optimal number for the algorithm “single linkage” could not be reached within 20 clusters compared with other algorithms, thus we eliminated it. For accuracy, we assessed the resulting dendrograms by the co-phenetic correlation coefficient (97), which showed how well the dendrograms represented the original data. Overall, UPGMA had the best performance (Table S7). We implemented all analyses in the R package *phyloregion* 1.0.6 (98).

To assess the occurrence of phylogenetic breaks at a finer taxonomic resolution, we computed phylogenetic regionalization for the top 20 families. Focusing on a number of clusters set to 10 for each family, we then counted the number of breaks (boundaries between clusters) along latitude (in 50-km intervals) occurring in the elevation band below or above 500 m. This analysis illustrated that some breaks along latitude occur in most families, and that some families show more composition splits along the escarpment. In addition, we computed an analysis matching the species level ranges to their phylogenetic position, using previously published maximum clade credibility trees (50, 54) from two clades (*Bullbophyllum*, *Dypsis*). We mapped the correspondence between the geographic ranges and the species position on the phylogeny (Figs. S16 and S17).

We fitted a random forest classification model to assess the performance of geographic and climatic variables in predicting the 10 biogeographic realms within the eastern escarpment of Madagascar (Fig. 4). We used the combination of elevation and latitude as proxies of topographic barriers along the escarpment. For climatic variables, we selected temperature seasonality, mean temperature of the coldest quarter, precipitation of the driest month, and site water balance (99) as four key predictors and paired them. We carried out all classifications using the R package *randomforest* 4.7-1(100). We implemented a stratified sampling method and sampled about one-third of the points within the escarpment regions. In total, we used 2,000 unique observations for the model. The number of variables to be considered for each split (*mtry*) is 1 and the forest size is 1,000 trees. The out-of-bag (OBB) error is an estimate of the error in the test set, which is calculated as a percentage of the number of misclassified samples divided by the number of the full sample set. We evaluated the performance of the models with different geological and climatic variables based on OBB error.

Mapping rarity of endemic species

Rare endemic species are expected to result from local origination, and thus their occurrence should be more connected to the geological processes shaping their speciation. The density distribution of rare species is expected to best highlight the area of intense activity that may result in the formation of new lineages. To identify the area of Madagascar that harbors the highest density of rare species, we mapped the locations of rare species within cells of 50 km × 50 km across the entire island. We controlled for variation in sampling effort by calculating both the Margalef and Menhinick indices (32), which assume that species richness (S) increases nonlinearly (nearly logarithmically or following a square-root function) with increasing sampling intensity (N):

$$S_{Margalef} = \frac{S - 1}{\ln N}$$

$$S_{Menhinick} = \frac{S}{\sqrt{N}}$$

654 We focused on the species with fewer than 20 observation records. For each 50 km × 50 km grid
655 cell, we calculated the total number of observations, as well as the total number of rare species. In
656 addition, we estimated the geographic extent of the locality where those rare species occur. For
657 species with more than one observation record, we calculated the average distance between
658 occurrences (Fig. S20).

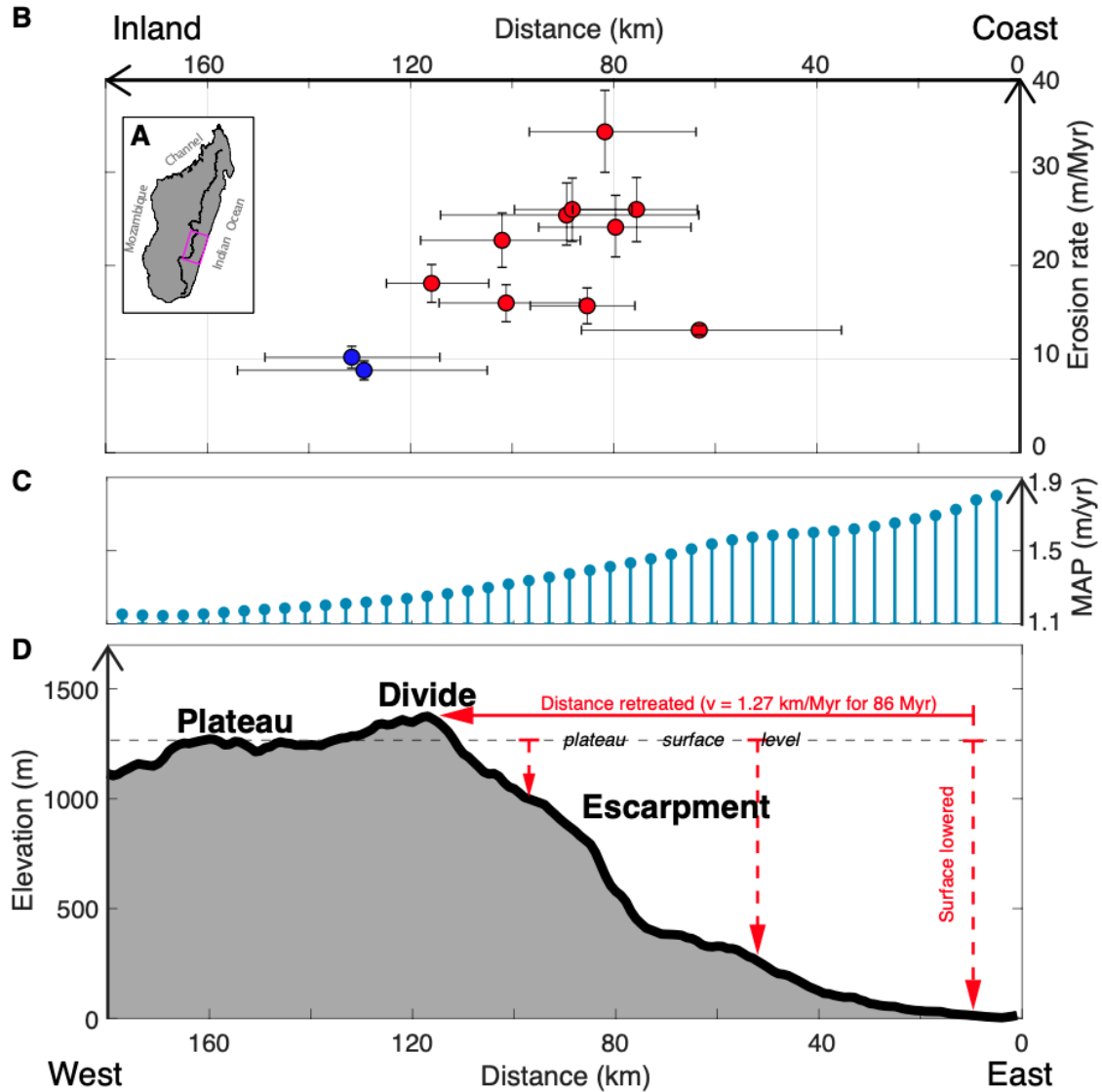


Fig. S1.

Topographical dynamics of an escarpment segment of Madagascar shown with multiple West-East oriented cross-sectional profiles starting from the coast. The island major divide is marked by the thick black line in (A). The mean topography inside of the magenta box is shown in (D). (B) Basin-wide erosion rates show that the plateau (the blue dots) is eroding systematically slower than the escarpment (the red dots), sustaining active retreat of the steep escarpment. Each dot represents a cosmogenic nuclide ^{10}Be basin where the lateral bar indicates the basin extent and the vertical bar indicates the standard deviation of erosion rate (18). (C) Mean annual precipitation (MAP) averaged from 2014 to 2018 [available at <https://pmm.nasa.gov/data-access/downloads/gpm>, (101)] The escarpment actively acts as an orographic barrier of precipitation. (D) The surface is substantially lowered due to the retreat on the escarpment since rifting. Modern escarpment location is consistent with constant retreat from the coast at the rate of 1.27 km/Myr since rifting, consistent with ^{10}Be estimates (18).

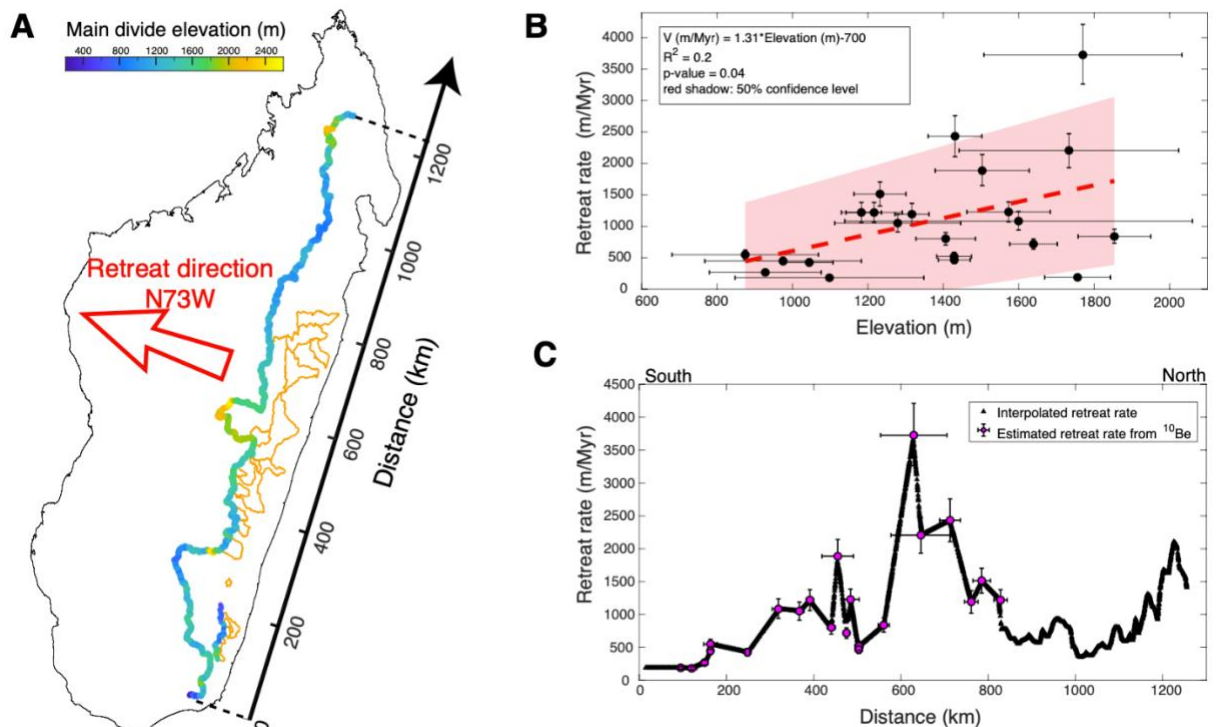
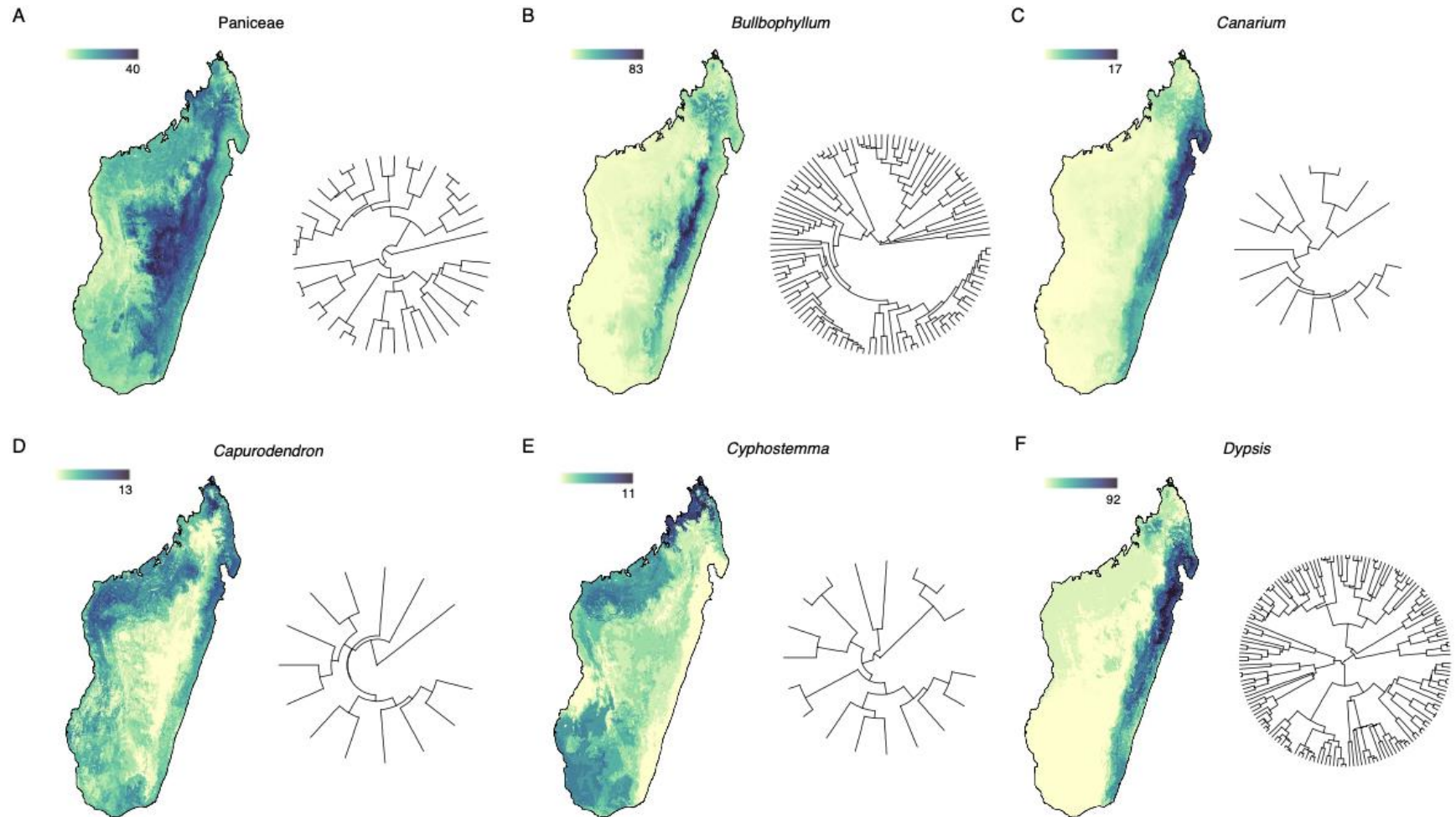


Fig. S2.

(A) The escarpment-divide topographic system of Madagascar extends along the eastern coastline over 1200 km. The major divide is marked with colored lines. The color indicates the divide height. Divide height is from SRTM-90m digital elevation model. The orange polygons indicate the escarpment-draining basins where the escarpment retreat rate is estimated with cosmogenic nuclide ^{10}Be concentrations (18). (B) Escarpment retreat rate measured by ^{10}Be concentrations and relationship to divide height. Retreat rates are from (18). Error bars indicate one standard deviation of plateau divide height and erosion rate for basin. Inset shows the statistics of the regression of retreat rate, V , against elevation of the data. (C) Measured (magenta circles) and interpolated (black triangles) escarpment retreat rates along the divide. In the southern 800 km, retreat rate is estimated from ^{10}Be data. North of the data, the scaling relationship from (B) is used to estimate the retreat rate.

686



687

688 **Fig. S3.**

689 Species richness maps of six clades (**A** Paniceae, **B** *Bullbophyllum*, **C** *Canarium*, **D** *Capurodendron*, **E** *Cyphostemma*, **F** *Dypsis*) and
 690 their maximum clade credibility (MCC) phylogenetic trees derived from (49 - 54).

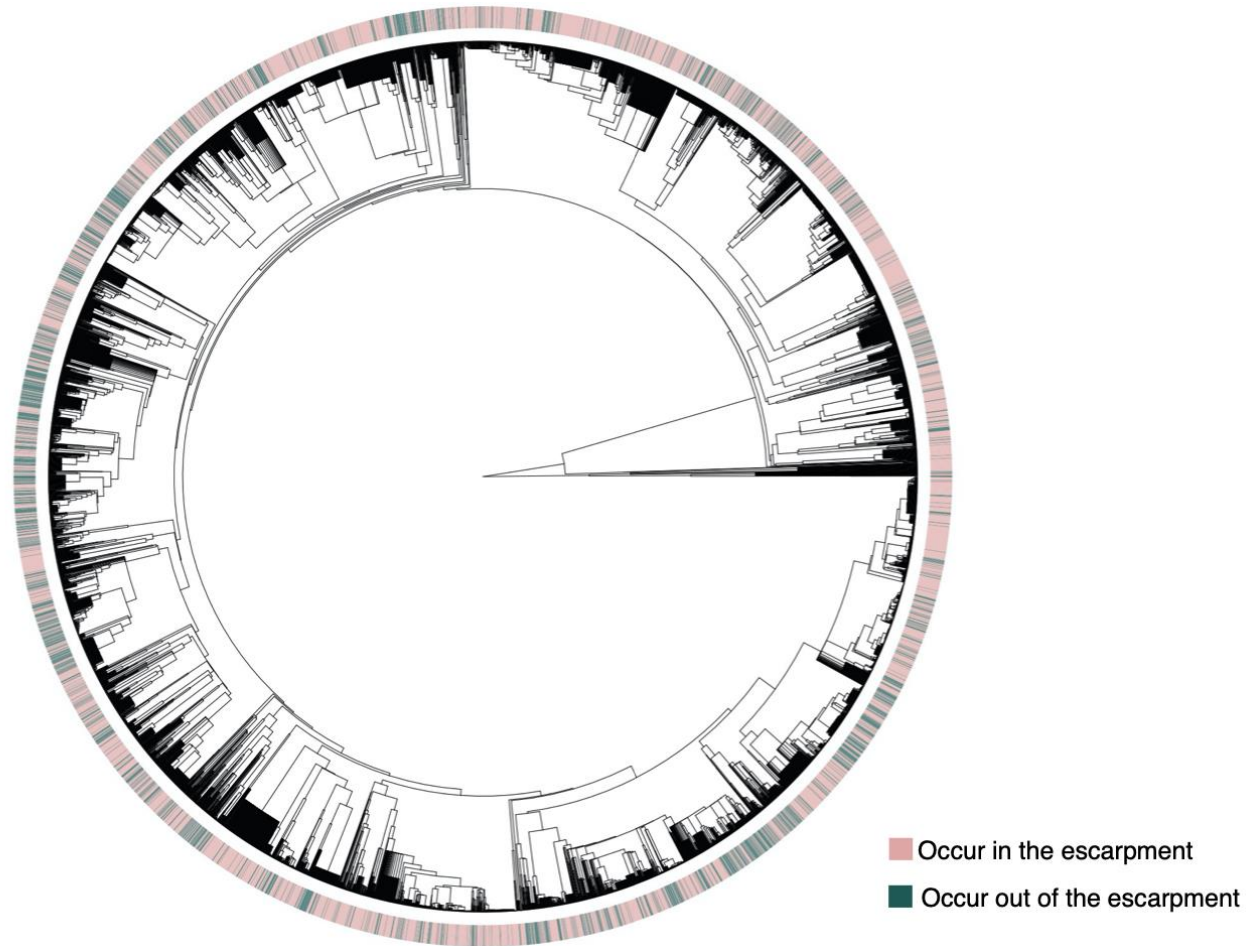
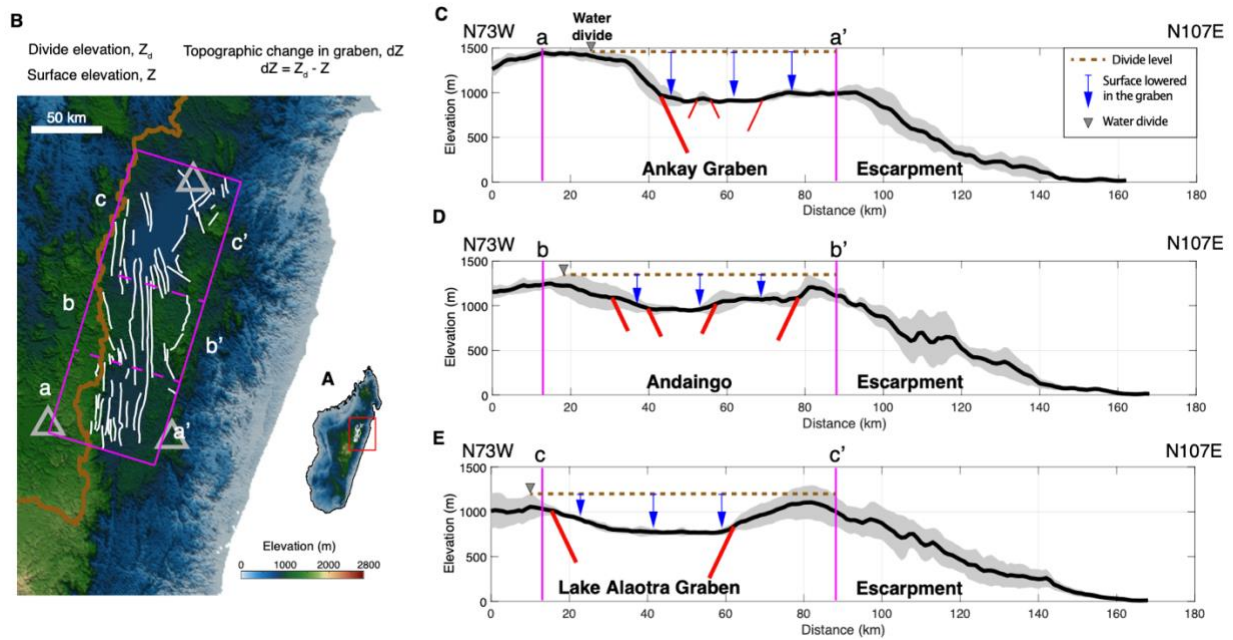


Fig. S4.

Distribution information of species on the phylogeny of 8,884 seed plants in Madagascar. We used a dated megaphylogeny for seed plants (25) as the backbone to generate the phylogeny. Colors mapped on the phylogenetic tree correspond to the distribution of the species. We determined the proportion of the species range that lies within the escarpment and set 5% of the species range as the threshold to define whether the species occur in the escarpment or not.

697

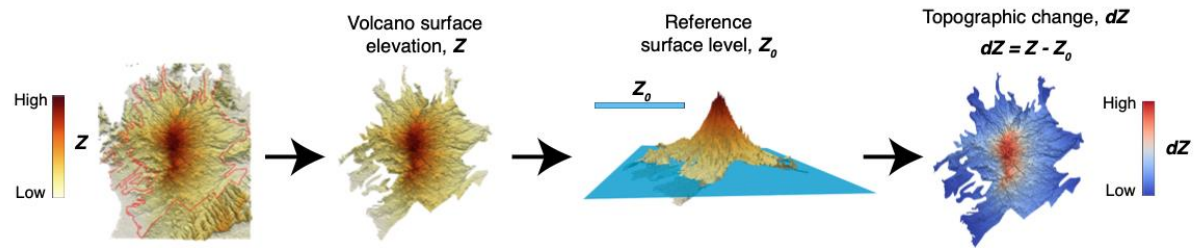


698

699 **Fig. S5.**

700 Surfaces of the Ankay-Alaotra Graben, differentially deformed from faulting. The location of the
 701 graben is indicated with the red box in (A) against the SRTM-90m digital elevation model in the
 702 background. (B) Topographic overview of the graben. Faults mapped by (22) are indicated with
 703 white lines. Triangles indicate locations of three exhumation ages of bedrock, all indicating little
 704 exhumation following rifting (21). The island's main divide is indicated with the thick brown line.
 705 The magenta box prescribes the mapped fault extents in space. (C–E) Topographic swath profiles
 706 of the three sub-domains of the graben. Dashed lines show the mean divide height of each sub-
 707 domain. The major faults are qualitatively shown with the red lines.

708



709

710 **Fig. S6.**

711 Diagram summarizing the calculation of topographic changes due to formation of volcanic edifices,
 712 using the major peak of the Montagne d'Ambre volcano as an example. Erupted volcanic material
 713 builds up the topography, with minor lowering of the local surface area. Only the surface mantled
 714 by igneous rock is considered to be affected. The red polygon in the left-most image marks the
 715 extent of the mapped igneous rock of the Montagne d'Ambre volcano.

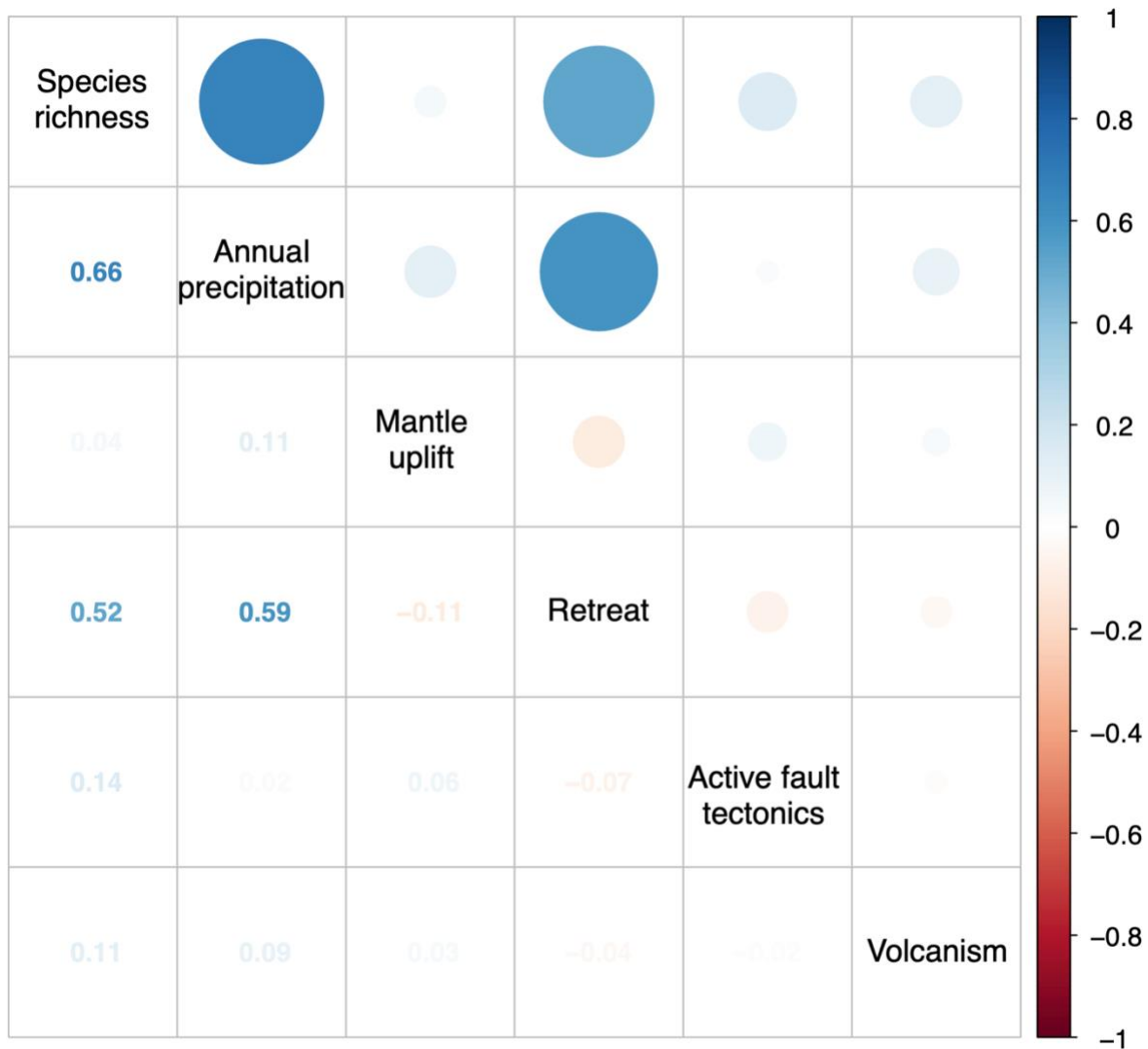


Fig. S7.

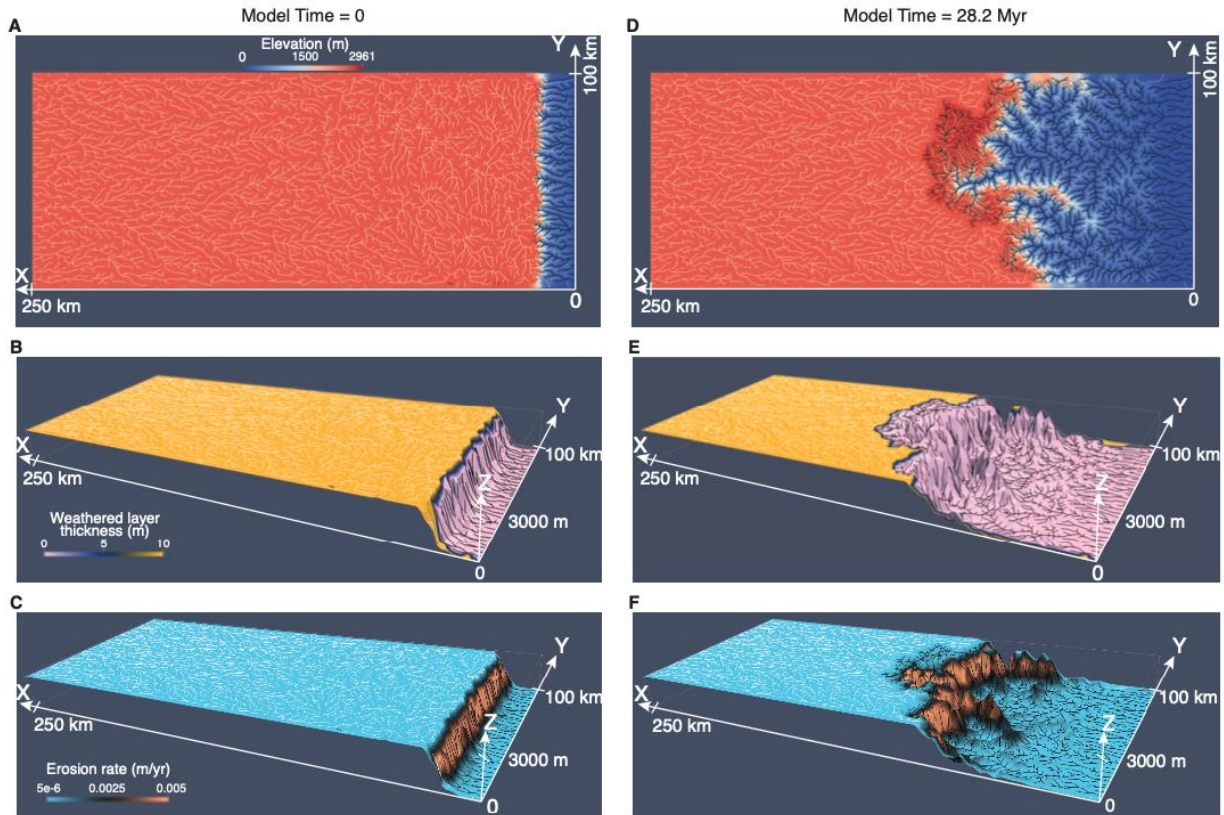
Spearman's correlation among species richness, annual precipitation and elevation change caused by four geological processes (mantle uplift, retreat, active fault tectonics, and volcanism; see Fig. 2). Retreat and annual precipitation are highly correlated, so the causal relationship with species richness is difficult to distinguish statistically.



Fig. S8.

Principal component analysis (PCA) plot showing the association between elevation change caused by four geological processes (mantle-derived uplift, escarpment retreat, active fault tectonics, and building of volcanic topography; see Fig. 2) as well as mean annual precipitation. Three regions, each dominated by one of these mechanisms are differentiated. Each symbol represents an area of 20×20 km. The axes (PC1, PC2) represent the two first principal components and explain 30.1% and 21.6% of the variance, respectively. Arrows in the plot represent the loadings, indicating the contribution of each original variable to the two first axes of the principal components (blue arrows underscore higher contributions). The colors of the scatter points represent the species richness and the symbols indicate the geographic area. Areas with highest species richness are found primarily in the east, where escarpment retreat is large and precipitation is high. A second region of high richness is in the north of the island, associated with high precipitation and mantle driven uplift. A global GLM considering these factors explains 51% of the variation.

738



739

740 **Fig. S9.**

741 Physical dynamics of the escarpment landscape evolution model, in the initial state (A–C) and at
 742 a model time of 28.2 Myr (D–F). (A, D) Map view of the escarpment topography and the river
 743 network. Escarpment rivers flow to the boundary $X = 0$ and are indicated with black lines. Plateau
 744 rivers flow to the boundary $X = 250$ km and are indicated with white lines. (B, E) Perspective view
 745 of the lithological differences, showing how the plateau is mantled by a more erodible, weathered
 746 layer while the escarpment domain is only bedrock. (C, F) Erosion is concentrated on the steep
 747 escarpment scarp.

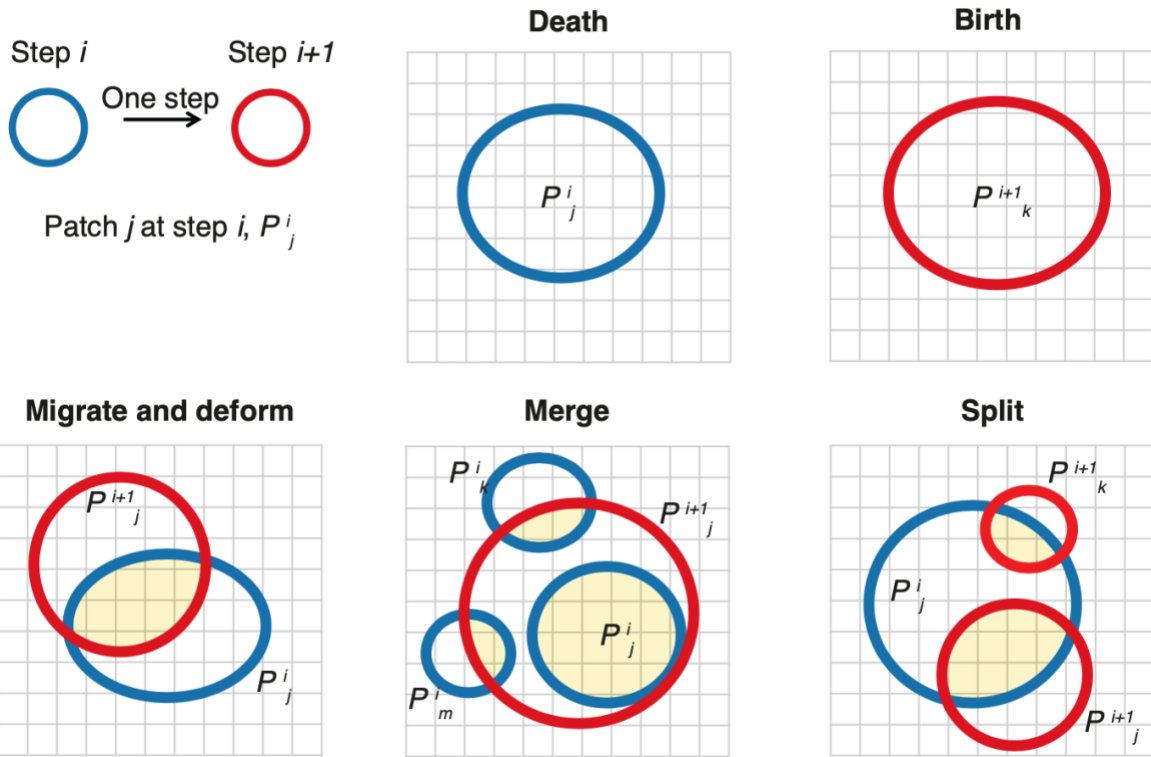
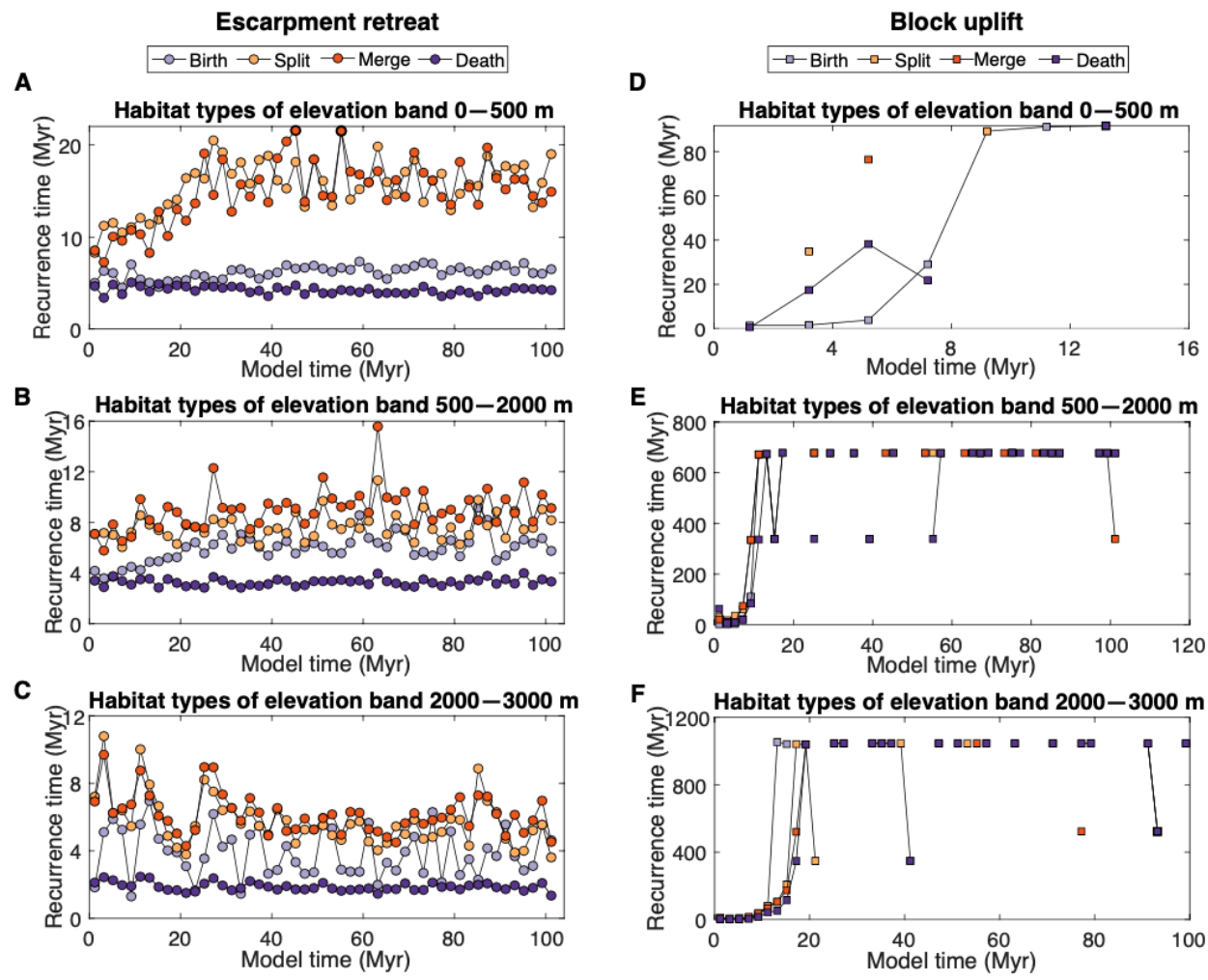


Fig. S10.

Illustration of multiple types of habitat patch change on a regular grid mesh. Blue and red circles indicate habitat patches of the same habitat type in two consecutive model steps. The area intersection of the blue and red patches is shown in yellow. Habitat patches are tracked throughout the model for each habitat type (Tables S5 and S6). Patches are labeled as P_j^i where the superscript, i , indicates the model steps, and the subscript (j,k,m) , indicates the patch index, which is unique to individual patches.

756



757

758 **Fig. S11.**

759 Average event recurrence time per habitat patch, separated by habitat type. Values are grouped
760 into three elevation bands for the escarment retreat model (A–C) and for the block uplift model
761 (D–F). Habitats are parametrically characterized by habitat model 1 (Table S5). Recurrence time
762 is averaged over a model time of 1 Myr. Discontinuous black lines in D–F indicate recurrence
763 times off the scale, as steady topography implies an infinite recurrence time.

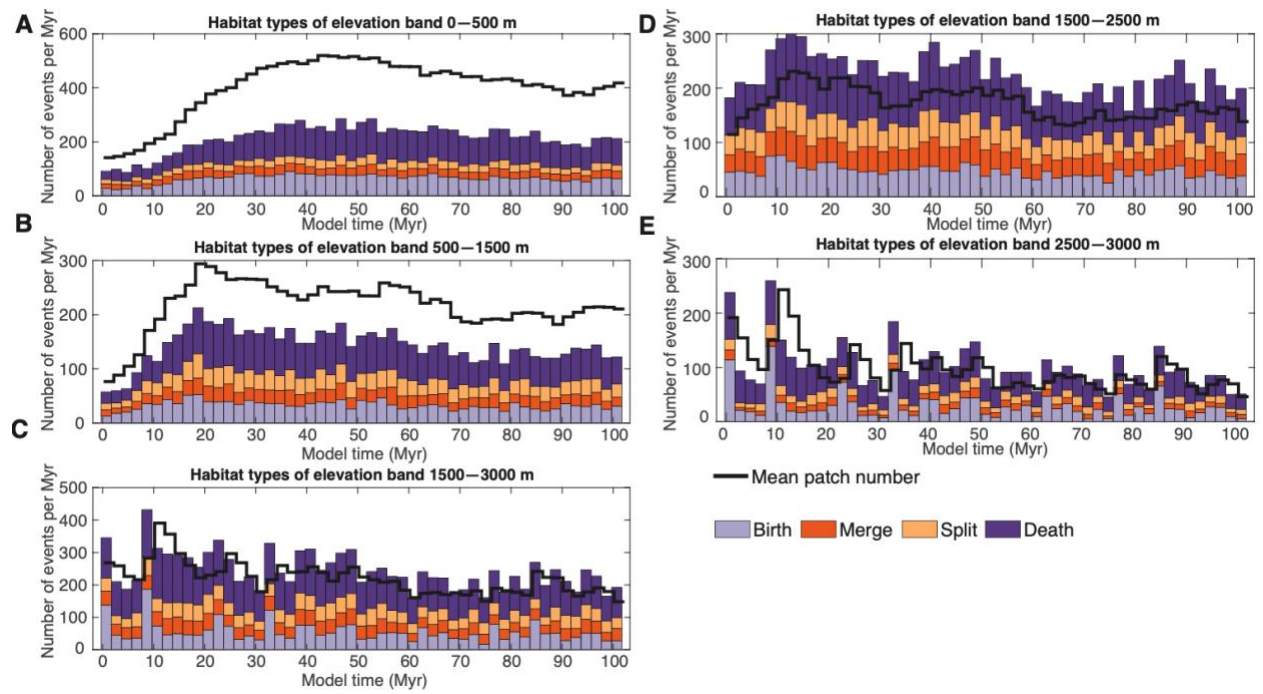


Fig. S12.

Frequency and types of habitat patch changes of the escarpment retreat model. Habitat types are parametrically defined with habitat model 2 as given in Table S6.

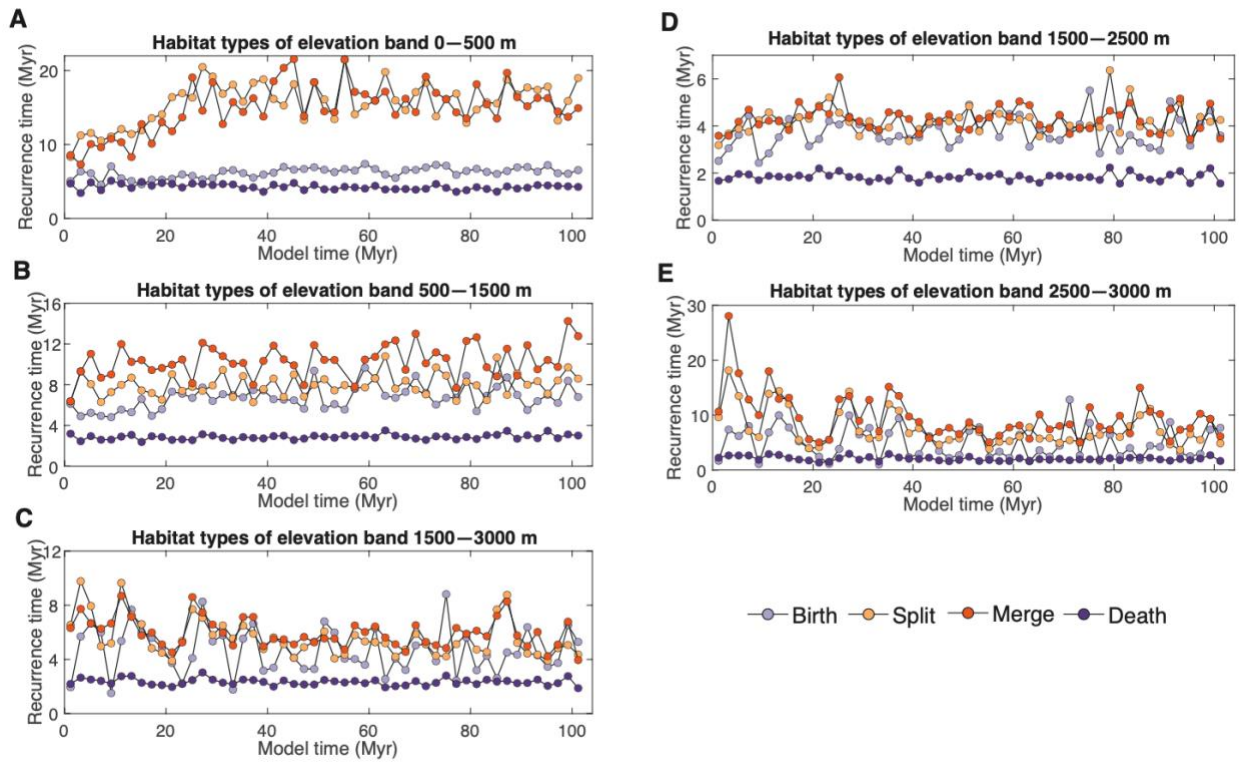


Fig. S13.

Average event recurrence time per habitat patch by habitat type, grouped into three elevation bands for the escarpment retreat model. Habitat types are parametrically defined by habitat model 2 in Table S6.

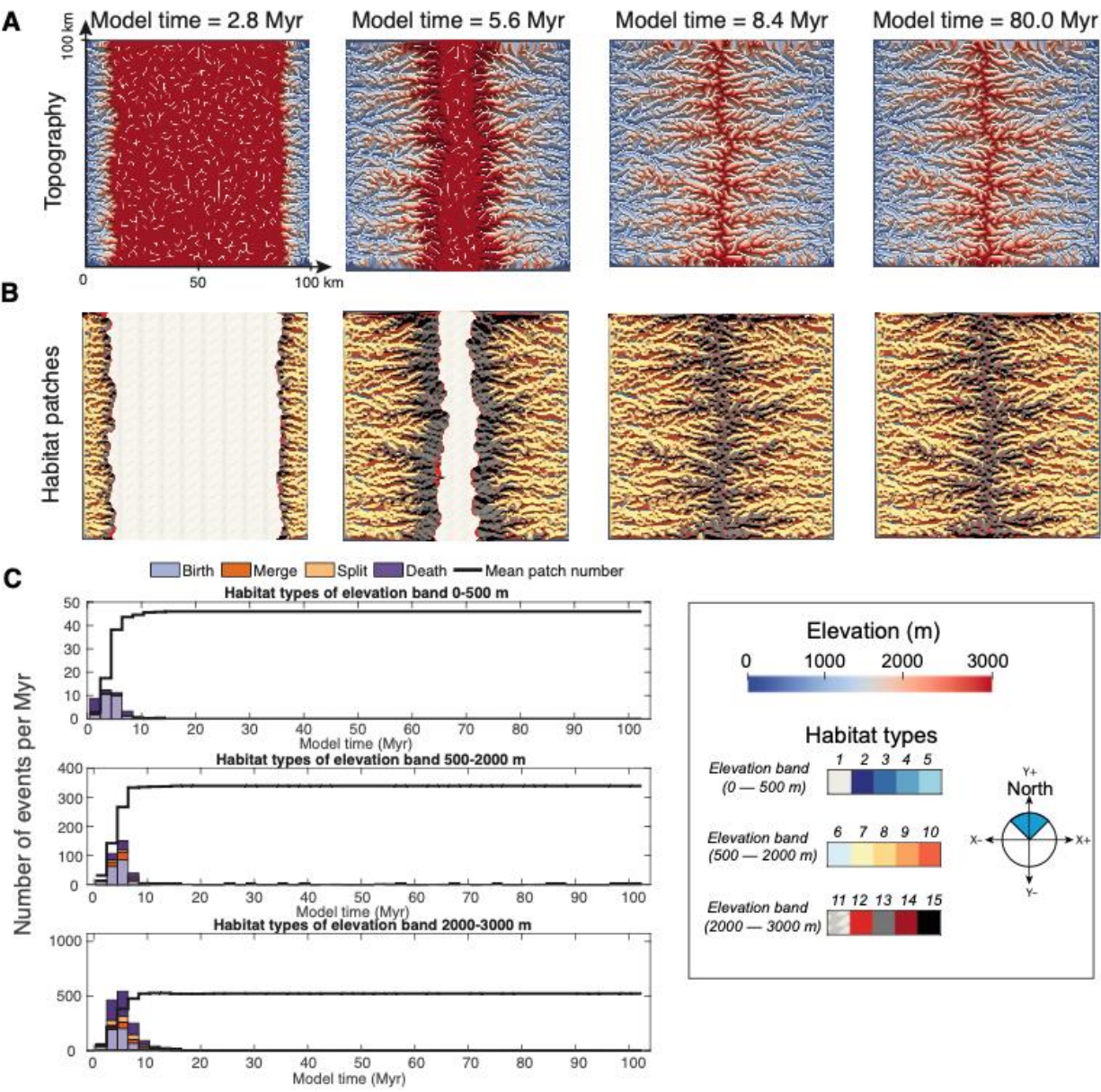


Fig. S14.

Topography and river network (white lines) for a landscape evolution model of a block uplift model in transient stages (model time 2.8, 5.6 and 8.4 Myr) and in a steady state (model time 80.0 Myr). The mountain range is symmetric, meaning that the major divide ridge is in the middle of the model domain ($X = 50$ km). See Table S3 for the model parameters. (B) Nominal habitat patches defined by elevation, slope and aspect (Table S5) of the time steps shown in (A). (C) The number of habitat patches and the frequency and types of patch evolution, grouped into habitat types of three elevation bands, as in Fig. 3.

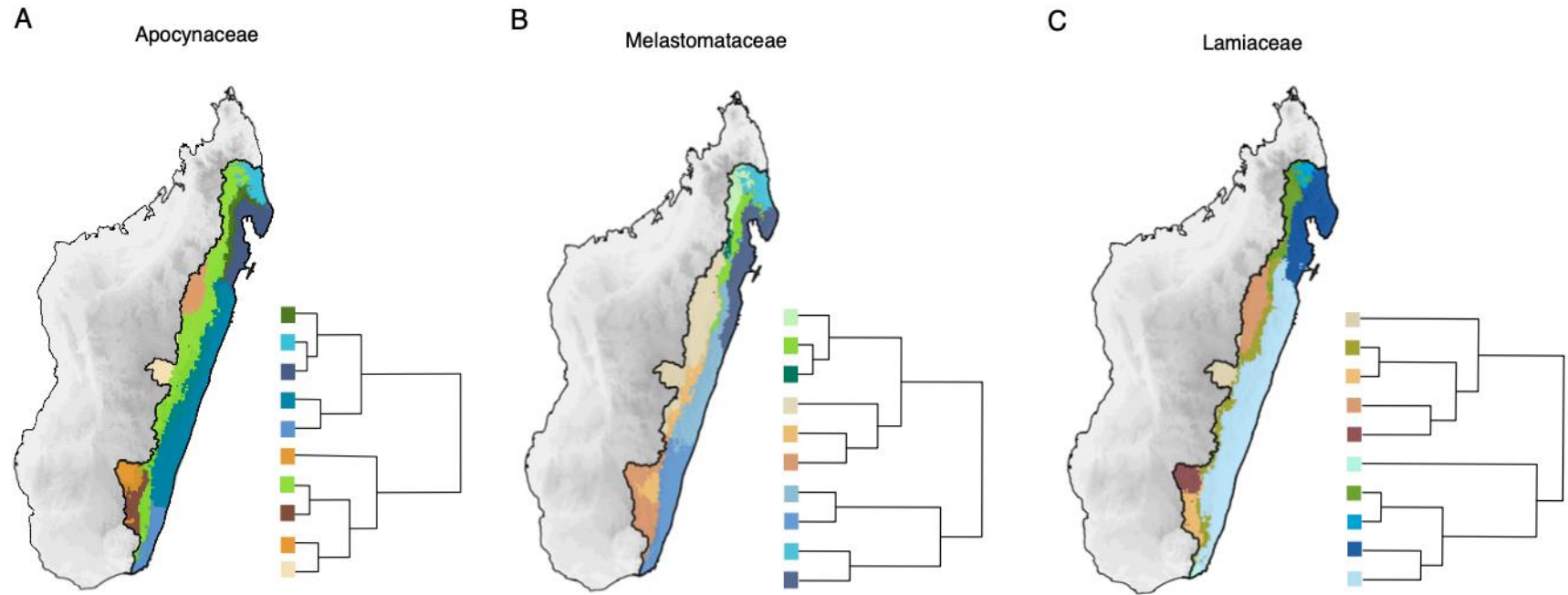
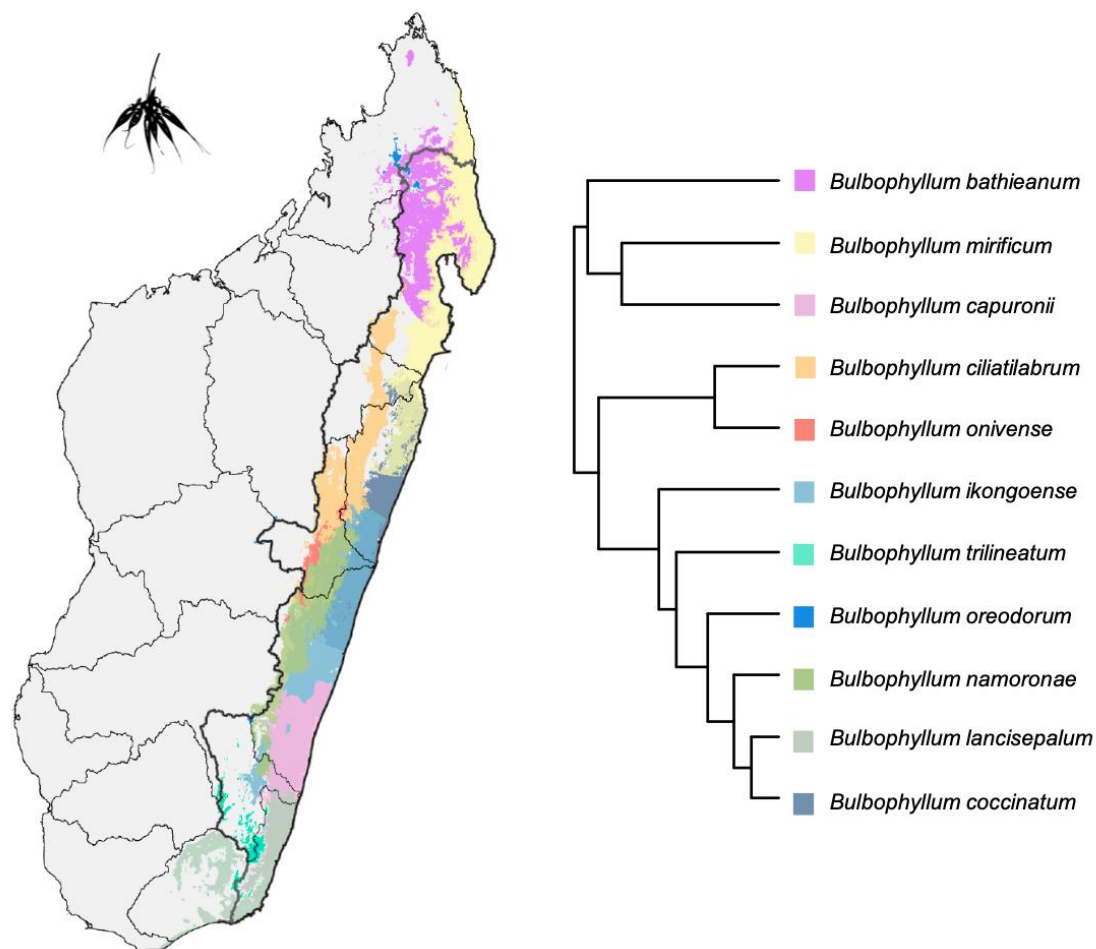


Fig. S15.

Distribution of the biogeographic realms (in distinct colors) for three example families (A, Apocynaceae; B, Melastomataceae; C, Lamiaceae) of plants in the escarpment based on phylogenetic turnover ($p\text{-}\beta\text{sim}$). $p\text{-}\beta\text{sim}$ were calculated using phylogenetic trees at family level and range maps of the species. Different families show distinct numbers and positions of biogeographic breaks.

791



792

793 **Fig. S16.**

794 Mapped species distribution along the escarpment within the clade *Bulbophyllum*. Range maps of the species were estimated using
 795 species distribution models with 1-km resolution. Phylogenetic relationships among species were extracted from the MCC tree (50).
 796 The background shows the major catchments and the dark north-south line is the main watersheds divide on the island.

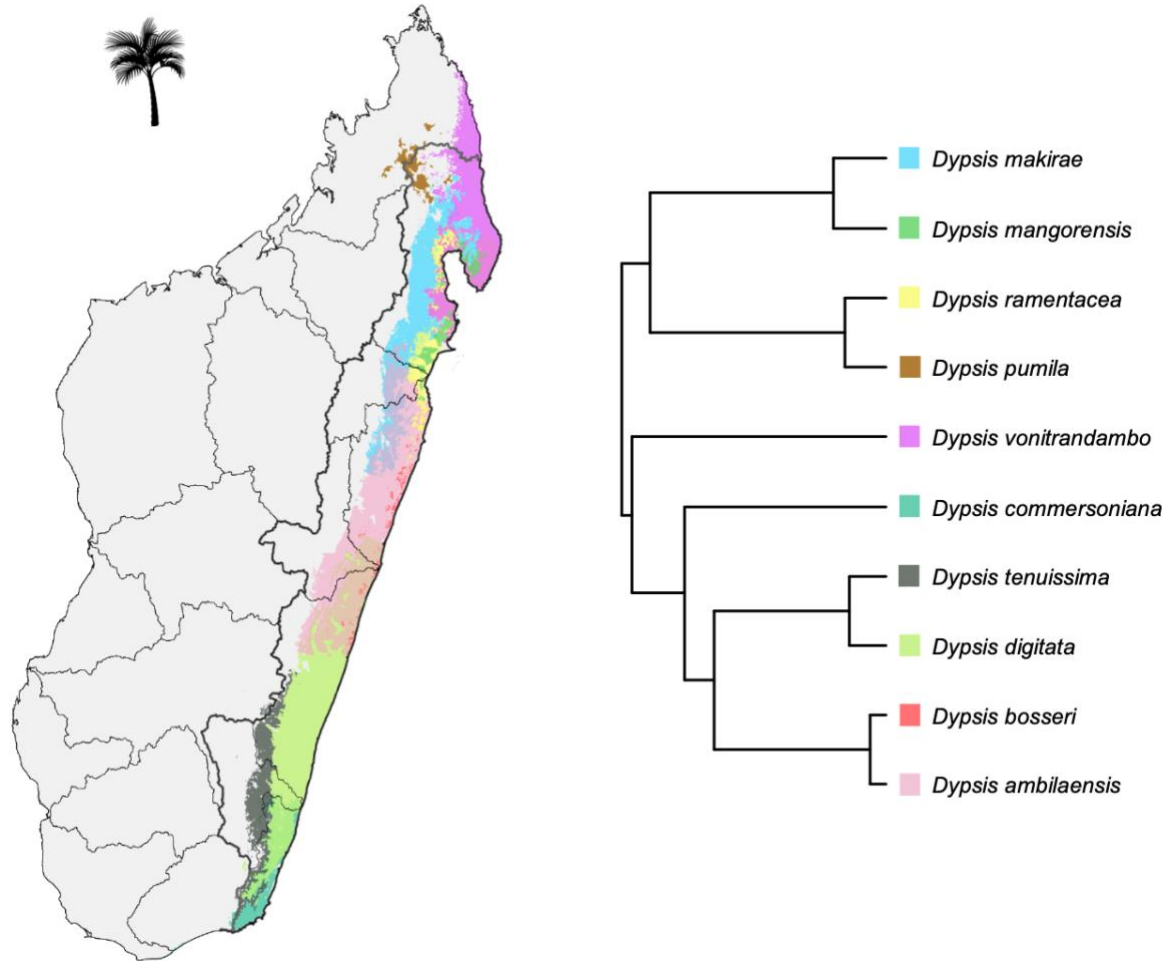


Fig. S17.

Mapped species distribution along the escarpment within the clade *Dypsis*. Range maps of the species were estimated using species distribution models with 1-km resolution. Phylogenetic relationships among species were extracted from the MCC tree (54). The background shows the major catchments and the dark north-south line is the main watersheds divide on the island.

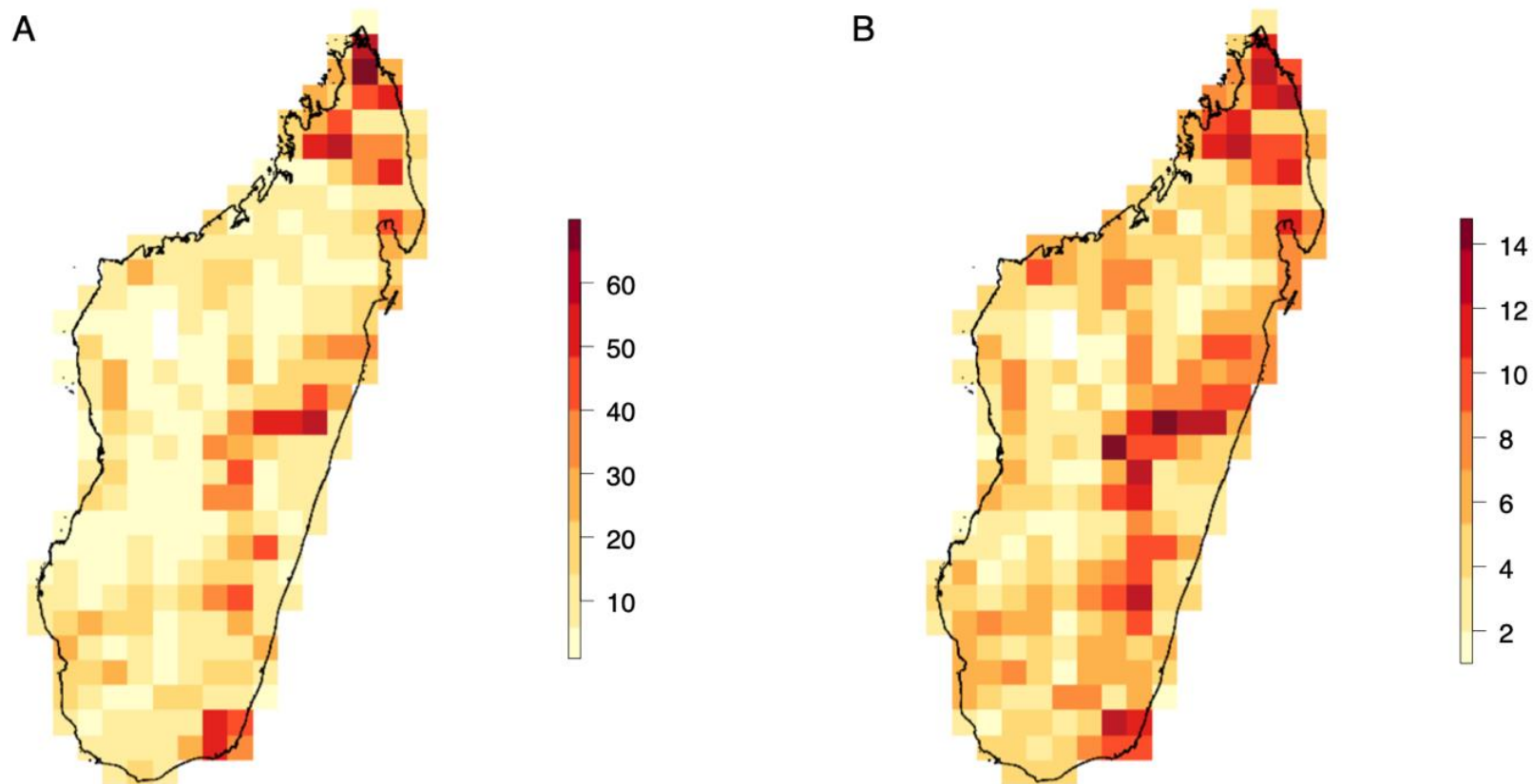
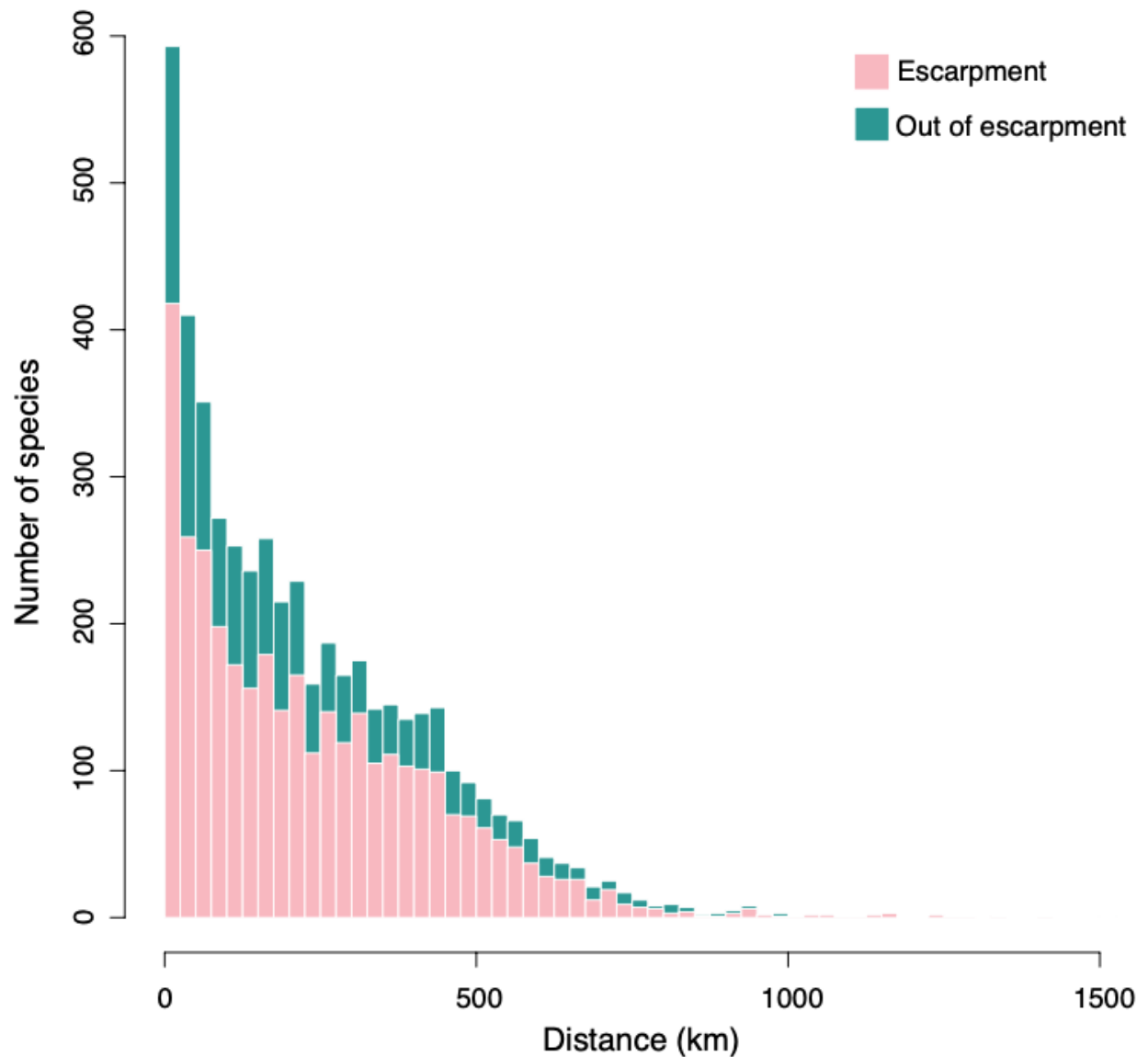


Fig. S18.

Maps of rarity of seed plant species in Madagascar at 50 km resolution. Colored cells correspond to areas with rare species (defined as fewer than 20 occurrences) rarified to the sampling intensity using the Margalef (A) and Menhinick (B) indices. The escarpment region of Madagascar has a high number of rare species compared to the western part.

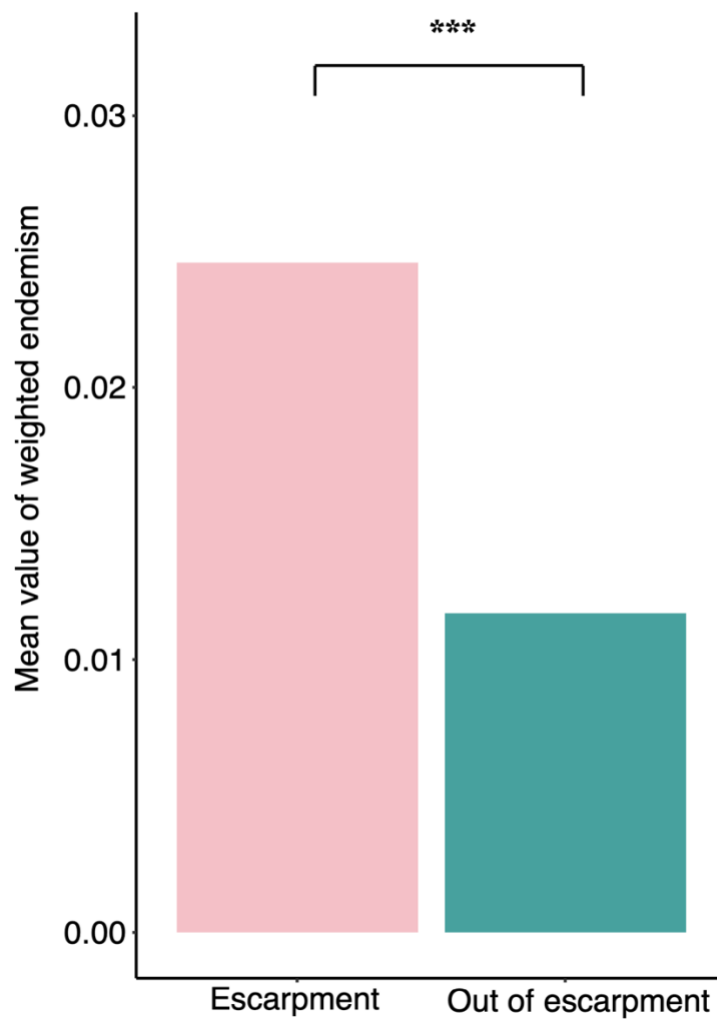
807
808



809

810 **Fig. S19.**

811 Histogram of average distances between documented occurrences of rare plant species in
812 Madagascar. Pink bars correspond to rare species in the escarpment region, while turquoise bars
813 correspond to rare species outside that region. The data demonstrate that the majority of these rare
814 species have a limited geographic range. Remarkably, 10% of these species have distances of less
815 than 25 km between occurrences.



816
817

818 **Fig. S20.**

819 Comparison of weighted endemism between escarpment and out of escarpment regions. We
 820 calculated the weighted endemism by summing the inverse of the number of grid cells occupied
 821 for species present in individual cells using species distribution maps. The mean value of weighted
 822 endemism is higher in the escarpment than outside it (Wilcoxon test: $P < 0.001$). This indicates
 823 that more narrow-ranged species are distributed in the escarpment.

Table S1.
 Descriptions of the six different birth–death models fitted to the six selected clades in
 Madagascar.

Type of model	Model description	Model equation	Number of parameters	Model acronym
Constant-rate models	Constant speciation and no extinction	$\lambda(t)=\lambda_0$ and $\mu(t)=0$	1	BCST
	Constant speciation and constant extinction	$\lambda(t) = \lambda_0$ and $\mu(t) = \mu_0$	2	BCSTDCST
	Speciation variable and no extinction	$\lambda(t) = \lambda_0 e^{\alpha t}$ and $\mu(t) = 0$	2	BTimeVar
Time-dependent models	Speciation variable and constant extinction	$\lambda(t) = \lambda_0 e^{\alpha t}$ and $\mu(t) = \mu_0$	3	BTimeVarDCST
	Constant speciation and variable extinction	$\lambda(t) = \lambda_0$ and $\mu(t) = \mu_0 e^{\beta t}$	3	BCSTDTimeVar
	Both speciation and extinction variable	$\lambda(t) = \lambda_0 e^{\alpha t}$ and $\mu(t) = \mu_0 e^{\beta t}$	4	BTimeVarDTimeVar

Table S2.

Results of all diversification analyses performed on the six selected clades. The table includes the model, the number of parameters in the model, the estimated log-likelihood (logL), the corrected Akaike information criterion (AICc) and the corresponding parameter estimates (λ_0 = speciation rate at present, α = parameter controlling the dependency of speciation rate on time, μ_0 = extinction rate at present, and β = parameter controlling the dependency of extinction rate on time). Some models show limited differences in AICc, and the best-fitting model is highlighted in bold.

Clade	Sample fraction	Crown age (Ma)	Model	NP	LogL	AICc	λ_0	α	μ_0	β
<i>Bullbophyllum</i>	0.62	12.7	BCST	1	-265.632	533.299	0.36	-	-	-
			BCSTDCST	2	-265.632	535.367	0.36	-	0	-
			BTimeVar	2	-265.616	535.334	0.37	- 0.006	-	-
			BTimeVarDCS T	3	-265.616	537.439	0.37	- 0.006	0	-
			BCSTDTimeVa r	3	-265.632	537.472	0.36	-	0	0.03
			BTimeVarDTim eVar	4	-265.616	539.58	0.37	- 0.006	0	0.05
<i>Canarium</i>	0.73	8.4	BCST	1	-36.547	75.38	0.23	-	-	-
			BCSTDCST	2	-36.547	78.017	0.235	-	0	-
			BTimeVar	2	-34.778	74.48	0.11	0.22	-	-
			BTimeVarDCS T	3	-34.779	77.557	0.11	0.22	0	-
			BCSTDTimeVa r	3	-36.547	81.094	0.23	-	0	0.00 5
			BTimeVarDTim eVar	4	-34.779	81.194	0.11	0.22	0	-0.11
<i>Capurodendron</i>	0.46	45.5	BCST	1	-43.857	90.114	0.05	-	-	-
			BCSTDCST	2	-43.857	93.047	0.05	-	0	-
			BTimeVar	2	-41.853	89.039	0.02	0.05	-	-
			BTimeVarDCS T	3	-41.853	92.705	0.02	0.05	0	-
			BCSTDTimeVa r	3	-43.857	96.714	0.05	-	0	0.02
			BTimeVarDTim eVar	4	-41.853	97.42	0.02	0.05	0	-0.01

<i>Cyphostemma</i>	0.62	32.8	BCST	1	-62.422	127.094	0.07	-	-	-
			BCSTDCST	2	-62.422	129.644	0.07	-	0	-
			BTimeVar	2	-61.539	127.878	0.04	0.03	-	-
			BTimeVarDCS T	3	-61.539	130.792	0.04	0.04	0	-
			BCSTDTimeVa r	3	-62.422	132.558	0.07	-	0	0.00 5
			BTimeVarDTim eVar	4	-61.539	134.155	0.04	0.04	0.03	0
<i>Dypsis</i>	0.94	13.5	BCST	1	-322.183	646.393	0.32	-	-	-
			BCSTDCST	2	-322.173	648.428	0.33	-	0.012	-
			BTimeVar	2	-322.152	648.385	0.33	- 0.007	-	-
			BTimeVarDCS T	3	-322.152	650.467	0.33	- 0.007	0	-
			BCSTDTimeVa r	3	-322.166	650.495	0.33	-	0.01	0.08
			BTimeVarDTim eVar	4	-322.152	652.578	0.33	- 0.007	0	0.03
Paniceae	0.28	25.6	BCST	1	-130.948	263.985	0.18	-	-	-
			BCSTDCST	2	-130.838	265.985	0.2	-	0.05	-
			BTimeVar	2	-130.879	266.065	0.18	- 0.009	-	-
			BTimeVarDCS T	3	-130.834	268.3	0.21	0.003	0.06	-
			BCSTDTimeVa r	3	-130.824	268.279	0.22	-	0.08	-0.04
			BTimeVarDTim eVar	4	-130.712	270.506	0.21	0.1	0.16	0.11

836 **Table S3.**
837 Parameters used in the landscape evolution models.

Category	Parameter	Symbol	Value	
			Escarpment retreat model	Block uplift model
Domain size	Length in X (east–west) direction	XL	250 km	100 km
	Length in Y (north–south) direction	YL	100 km	100 km
	Plateau height	Zp	2600 m	Not applicable
Numerical	Timestep	dt	2000 years	2000 years
Erosion laws	Stream power law slope exponent	n	1	1
	Stream power law discharge exponent	m	0.495	0.495
	Inverse Hack’s law power	H	2	2
	Inverse Hack’s law coefficient	ka	1.66667	1.66667
	Critical hillslope length	Xc	1000 m	1400 m
	Critical hillslope angle	$theta$	21°	45°
	Hillslope diffusivity	Kf	0.007 m ² /yr	0.007 m ² /yr
	Fresh bedrock erodibility	Kb	0.00000025 m ^{0.2} /yr	0.0000035 m ^{0.2} /yr
External forcing	Precipitation rate	p	1 m/yr	1 m/yr
	Uniform uplift rate	U	0.0000005 m/yr	0.0022 m/yr
Weak weathering layer	Thickness	Thw	10 m	Not applicable
	Erodibility	Kw	0.000025 m ^{0.2} /yr	Not applicable

838 **Table S4.**
839 Performance of predictors in the random forest classification model explaining the distribution of
840 biogeographic realms.

Category	Predictor(s)	Out-of-bag error rate (OOB)
Geological dynamics	elevation + latitude	13.88%
Climate	temperature seasonality + mean temperature of coldest quarter	29.86%
	temperature seasonality + precipitation of driest month	34..92%
	temperature seasonality + site water balance	35.12%
	mean temperature of coldest quarter + precipitation of driest month	36.72%
	mean temperature of coldest quarter + site water balance	38.93%
	precipitation of driest month + site water balance	45.44%

841

842 **Table S5.**

843 Parameters for habitat model 1 in the physiographic analysis of landscape evolution models.

Habitat type	Elevation (m)	Hillslope aspect facing north	Hillslope gradient (degrees)
1	0—500	no	0—3
	0—500	yes	0—3
2	0—500	no	3—20
3	0—500	no	>20
4	0—500	yes	3—20
5	0—500	yes	>20
6	500—2000	no	0—3
	500—2000	yes	0—3
7	500—2000	no	3—20
8	500—2000	no	>20
9	500—2000	yes	3—20
10	500—2000	yes	>20
11	2000—3000	no	0—3
	2000—3000	yes	0—3
12	2000—3000	no	3—20
13	2000—3000	no	>20
14	2000—3000	yes	3—20
15	2000—3000	yes	>20

844

845 **Table S6.**
846 Parameters for habitat model 2 in the physiographic analysis of landscape evolution models.

Habitat type	Elevation (m)	Hillslope aspect facing north	Hillslope gradient (degrees)
1	0—500	no	0—3
	0—500	yes	0—3
2	0—500	no	3—20
3	0—500	no	>20
4	0—500	yes	3—20
5	0—500	yes	S>20
6	500—1500	no	0—3
	500—1500	yes	0—3
7	500—1500	no	3—20
8	500—1500	no	>20
9	500—1500	yes	3—20
10	500—1500	yes	>20
11	1500—2500	no	0—3
	1500—2500	yes	0—3
12	1500—2500	no	3—20
13	1500—2500	no	>20
14	1500—2500	yes	3—20

15	1500—2500	yes	>20
16	2500—3000	no	0—3
	2500—3000	yes	0—3
17	2500—3000	no	3—20
18	2500—3000	no	>20
19	2500—3000	yes	3—20
20	2500—3000	yes	>20
21	1500—3000	no	0—3
	1500—3000	yes	0—3
22	1500—3000	no	3—20
23	1500—3000	no	>20
24	1500—3000	yes	3—20
25	1500—3000	yes	>20

Table S7.

Summary of performance among statistical approaches eight algorithms [single linkage, complete linkage, unweighted pair group method with arithmetic mean (UPGMA), unweighted pair group method using centroids (UPGMC), weighted pair group method with arithmetic mean (WPGMA), weighted pair group method using centroids (WPGMC), and Ward's minimum variance criterion (Ward's D) and its modification (Ward's D2)] considered for clustering species assemblages into phylogenetic regions based on phylogenetic beta diversity values.

Algorithm	Optimal k	Explained variance (k_{op})	Co-phenetic correlation coefficient
UPGMA	10	0.81	0.73
Ward's D	12	0.85	0.72
Ward's D2	13	0.85	0.71
WPGMA	15	0.81	0.62
WPGMC	18	0.77	0.58
UPGMC	20	0.78	0.50
complete	15	0.82	0.63
single	>20	-	-

Movie S1.

Dynamics of escarpment retreat from the *DAC* landscape evolution model from three perspectives. Frame A (top left) is a perspective view of erosion rate showing the high rates on the steep escarpment, contrasting with the slowly eroding high plateau. The differential erosion rate of the two topographical domains drives the escarpment to retreat inland. Frame B (bottom left) shows the map view of elevation change during retreat. An elevation band of 1000-1500 m is highlighted with yellow to qualitatively show the emergence, fragmentation, and isolation of a characteristic elevation band. Frame C (right) is a perspective view of the model showing the heterogeneous retreat by highlighting three escarpment catchments as discussed in main text (green, blue, and orange). Model time is shown in Frame C.

Movie S2.

Habitat distribution for the escarpment retreat model. Habitat types are parametrically defined by elevation, hillslope aspect, and hillslope gradient (Table S5). Habitat type 1 and 11 are the flat coastal plain and the high plateau, respectively. The other habitat types are from different elevation bands on the escarpment. Leftward retreat of the escarpment creates isolated habitat patches in the valleys and on the ridges.

Movie S3.

Habitat patch geometry change for one habitat type of the escarpment retreat model during model time of 50 -60 Myr. Patches shown are from the habitat type that is parameterized with elevation (1500-2500 m), hillslope gradient (3-20 degree), and slope aspect (not facing north)(Table S6). Birth, deformation, splitting, and merging of patches are colored. During the westward retreat of the escarpment, habitat patches change shape, area and number.

Movie S4.

Topographic evolution of a block uplift model with two frames. The left frame shows the topography (colored background) and the river network (white lines). The right frame shows the erosion rate. The block is homogeneously uplifted at a constant rate. After a transient stage of about 8 Myrs, the topography reaches a steady state where the major water divide is in the middle of the block, separating the left- and right- flowing river networks. At steady state, river network geometry is unchanging and erosion rate is uniform and equal to the uplift rate. Model time is shown in the left frame.

886 References and Notes

- 887 1. A. Antonelli, R. J. Smith, A. L. Perrigo, A. Crottini, J. Hackel, W. Testo, H. Farooq, M. F.
888 Torres Jiménez, N. Andela, T. Andermann, A. M. Andriamanohera, S. Andriambololonera, S. P.
889 Bachman, C. D. Bacon, W. J. Baker, F. Belluardo, C. Birkinshaw, J. S. Borrell, S. Cable, N. A.
890 Canales, J. D. Carrillo, R. Clegg, C. Clubbe, R. S. C. Cooke, G. Damasco, S. Dhanda, D. Edler,
891 S. Faurby, P. de Lima Ferreira, B. L. Fisher, F. Forest, L. M. Gardiner, S. M. Goodman, O. M.
892 Grace, T. B. Guedes, M. C. Henniges, R. Hill, C. E. R. Lehmann, P. P. Lowry 2nd, L. Marline,
893 P. Matos- Maraví, J. Moat, B. Neves, M. G. C. Nogueira, R. E. Onstein, A. S. T. Papadopoulos,
894 O. A. Perez-Escobar, L. N. Phelps, P. B. Phillipson, S. Pironon, N. A. S. Przelomska, M.
895 Rabarimanarivo, D. Rabehevitra, J. Raharimampionona, M. T. Rajaonah, F. Rajaonary, L. R.
896 Rajaovelona, M. Rakotoarinivo, A. A. Rakotoarisoa, S. E. Rakotoarisoa, H. N. Rakotomalala, F.
897 Rakotonasolo, B. A. Ralaiveloarisoa, M. Ramirez-Herranz, J. E. N. Randriamamonjy, T.
898 Randriamboavonjy, V. Randrianasolo, A. Rasolohery, A. N. Ratsifandrihamanana, N.
899 Ravololomanana, V. Razafiniary, H. Razanajatovo, E. Razanatsoa, M. Rivers, F. Sayol, D.
900 Silvestro, M. S. Vorontsova, K. Walker, B. E. Walker, P. Wilkin, J. Williams, T. Ziegler, A.
901 Zizka, H. Ralimanana, Madagascar's extraordinary biodiversity: Evolution, distribution, and use.
902 *Science* **378**, eabf0869 (2022). doi:10.1126/science.abf0869 Medline
- 903 2. M. Vences, K. C. Wollenberg, D. R. Vieites, D. C. Lees, Madagascar as a model region of
904 species diversification. *Trends Ecol. Evol.* **24**, 456–465 (2009). doi:10.1016/j.tree.2009.03.011
905 Medline
- 906 3. M. J. de Wit, Madagascar: Heads it's a continent, tails it's an island. *Annu. Rev. Earth Planet.*
907 *Sci.* **31**, 213–248 (2003). doi:10.1146/annurev.earth.31.100901.141337
- 908 4. A. D. Gibbons, J. M. Whittaker, R. D. Müller, The breakup of East Gondwana: Assimilating
909 constraints from Cretaceous ocean basins around India into a best-fit tectonic model. *J. Geophys.*
910 *Res. Solid Earth* **118**, 808–822 (2013). doi:10.1002/jgrb.50079
- 911 5. A. Crottini, O. Madsen, C. Poux, A. Strauss, D. R. Vieites, M. Vences, Vertebrate time- tree
912 elucidates the biogeographic pattern of a major biotic change around the K–T boundary in
913 Madagascar. *Proc. Natl. Acad. Sci. U.S.A.* **109**, 5358–5363 (2012).
914 doi:10.1073/pnas.1112487109 Medline
- 915 6. L. Wilmé, S. M. Goodman, J. U. Ganzhorn, Biogeographic evolution of Madagascar's
916 microendemic biota. *Science* **312**, 1063–1065 (2006). doi:10.1126/science.1122806 Medline
- 917 7. N. A. Wells, in *The Natural History of Madagascar*, S. M. Goodman, J. P. Benstead, Eds.
918 (Univ. of Chicago Press, 2003), pp. 16–34.
- 919 8. A. D. Yoder, C. R. Campbell, M. B. Blanco, M. Dos Reis, J. U. Ganzhorn, S. M. Goodman, K.
920 E. Hunnicutt, P. A. Larsen, P. M. Kappeler, R. M. Rasoloarison, J. M. Ralison, D. L. Swofford,
921 D. W. Weisrock, Geogenetic patterns in mouse lemurs (genus *Microcebus*) reveal the ghosts of
922 Madagascar's forests past. *Proc. Natl. Acad. Sci. U.S.A.* **113**, 8049–8056 (2016).
923 doi:10.1073/pnas.1601081113 Medline
- 924 9. J. L. Younger, P. Dempster, Á. S. Nyári, T. O. Helms, M. J. Raherilalao, S. M. Goodman, S.
925 Reddy, Phylogeography of the Rufous Vanga and the role of bioclimatic transition zones in

926 promoting speciation within Madagascar. *Mol. Phylogenet. Evol.* **139**, 106535 (2019).
 927 [doi:10.1016/j.ympev.2019.106535](https://doi.org/10.1016/j.ympev.2019.106535) Medline

928 10. S. M. Goodman, J. U. Ganzhorn, Biogeography of lemurs in the humid forests of
 929 Madagascar: The role of elevational distribution and rivers. *J. Biogeogr.* **31**, 47–55 (2004).
 930 [doi:10.1111/j.1365-2699.2004.00953.x](https://doi.org/10.1111/j.1365-2699.2004.00953.x)

931 11. C. Badgley, T. M. Smiley, R. Terry, E. B. Davis, L. R. G. DeSantis, D. L. Fox, S. S. B.
 932 Hopkins, T. Jezkova, M. D. Matocq, N. Matzke, J. L. McGuire, A. Mulch, B. R. Riddle, V. L.
 933 Roth, J. X. Samuels, C. A. E. Strömberg, B. J. Yanites, Biodiversity and topographic complexity:
 934 Modern and geohistorical perspectives. *Trends Ecol. Evol.* **32**, 211–226 (2017).
 935 [doi:10.1016/j.tree.2016.12.010](https://doi.org/10.1016/j.tree.2016.12.010) Medline

936 12. P. Descombes, T. Gaboriau, C. Albouy, C. Heine, F. Leprieur, L. Pellissier, Linking species
 937 diversification to palaeo-environmental changes: A process-based modelling approach. *Glob.*
 938 *Ecol. Biogeogr.* **27**, 233–244 (2018). [doi:10.1111/geb.12683](https://doi.org/10.1111/geb.12683)

939 13. C. Hoorn, V. Mosbrugger, A. Mulch, A. Antonelli, Biodiversity from mountain building.
 940 *Nat. Geosci.* **6**, 154 (2013). [doi:10.1038/ngeo1742](https://doi.org/10.1038/ngeo1742)

941 14. A. Antonelli, W. D. Kissling, S. G. A. Flantua, M. A. Bermúdez, A. Mulch, A. N. Muellner-
 942 Riehl, H. Kreft, H. P. Linder, C. Badgley, J. Fjeldså, S. A. Fritz, C. Rahbek, F. Herman, H.
 943 Hooghiemstra, C. Hoorn, Geological and climatic influences on mountain biodiversity. *Nat.*
 944 *Geosci.* **11**, 718–725 (2018). [doi:10.1038/s41561-018-0236-z](https://doi.org/10.1038/s41561-018-0236-z)

945 15. C. Rahbek, M. K. Borregaard, A. Antonelli, R. K. Colwell, B. G. Holt, D. Nogues-Bravo, C.
 946 M. Ø. Rasmussen, K. Richardson, M. T. Rosing, R. J. Whittaker, J. Fjeldså, Building mountain
 947 biodiversity: Geological and evolutionary processes. *Science* **365**, 1114–1119 (2019).
 948 [doi:10.1126/science.aax0151](https://doi.org/10.1126/science.aax0151) Medline

949 16. J. O. Thompson, M. Moulin, D. Aslanian, P. De Clarens, F. Guillocheau, New starting point
 950 for the Indian Ocean: Second phase of breakup for Gondwana. *Earth Sci. Rev.* **191**, 26–56
 951 (2019). [doi:10.1016/j.earscirev.2019.01.018](https://doi.org/10.1016/j.earscirev.2019.01.018)

952 17. A. Gilchrist, M. Summerfield, Differential denudation and flexural isostasy in formation of
 953 rifted-margin upwarps. *Nature* **346**, 739–742 (1990). [doi:10.1038/346739a0](https://doi.org/10.1038/346739a0)

954 18. Y. Wang, S. D. Willett, D. Wu, N. Haghipour, M. Christl, Retreat of the great escarpment of
 955 Madagascar from geomorphic analysis and cosmogenic ¹⁰Be concentrations. *Geochem. Geophys.*
 956 *Geosyst.* **22**, e2021GC009979 (2021). [doi:10.1029/2021GC009979](https://doi.org/10.1029/2021GC009979)

957 19. G. G. Roberts, J. D. Paul, N. White, J. Winterbourne, Temporal and spatial evolution of
 958 dynamic support from river profiles: A framework for Madagascar. *Geochem. Geophys. Geosyst.*
 959 **13**, Q04004 (2012). [doi:10.1029/2012GC004040](https://doi.org/10.1029/2012GC004040)

960 20. S. N. Stephenson, N. J. White, T. Li, L. F. Robinson, Disentangling interglacial sea level and
 961 global dynamic topography: Analysis of Madagascar. *Earth Planet. Sci. Lett.* **519**, 61–69 (2019).
 962 [doi:10.1016/j.epsl.2019.04.029](https://doi.org/10.1016/j.epsl.2019.04.029)

21. S. N. Stephenson, N. J. White, A. Carter, D. Seward, P. W. Ball, M. Klöcking, Cenozoic dynamic topography of Madagascar. *Geochem. Geophys. Geosyst.* **22**, e2020GC009624 (2021). doi:10.1029/2020GC009624
22. T. M. Kusky, E. Toraman, T. Raharimahefa, C. Rasoazanamparany, Active tectonics of the Alaotra-Ankay Graben System, Madagascar: Possible extension of Somalian- African diffusive plate boundary? *Gondwana Res.* **18**, 274–294 (2010). doi:10.1016/j.gr.2010.02.003
23. M. Mietton, Y. Gunnell, G. Nicoud, L. Ferry, R. Razafimahefa, P. Grandjean, ‘Lake’ Alaotra, Madagascar: A late Quaternary wetland regulated by the tectonic regime. *Catena* **165**, 22–41 (2018). doi:10.1016/j.catena.2018.01.021
24. Y. Wang, S. D. Willett, D. Wu, The role of weathering on morphology and rates of escarpment retreat of the rift margin of Madagascar. *J. Geophys. Res. Earth Surf.* **128**, e2022JF007001 (2023). doi:10.1029/2022JF007001
25. S. A. Smith, J. W. Brown, Constructing a broadly inclusive seed plant phylogeny. *Am. J. Bot.* **105**, 302–314 (2018). doi:10.1002/ajb2.1019 Medline
26. Y. Xing, R. H. Ree, Uplift-driven diversification in the Hengduan Mountains, a temperate biodiversity hotspot. *Proc. Natl. Acad. Sci. U.S.A.* **114**, E3444–E3451 (2017). doi:10.1073/pnas.1616063114 Medline
27. L. Goren, S. D. Willett, F. Herman, J. Braun, Coupled numerical–analytical approach to landscape evolution modeling. *Earth Surf. Process. Landf.* **39**, 522–545 (2014). doi:10.1002/esp.3514
28. J. Braun, A review of numerical modeling studies of passive margin escarpments leading to a new analytical expression for the rate of escarpment migration velocity. *Gondwana Res.* **53**, 209–224 (2018). doi:10.1016/j.gr.2017.04.012
29. S. D. Willett, S. W. McCoy, H. W. Beeson, Transience of the North American High Plains landscape and its impact on surface water. *Nature* **561**, 528–532 (2018). doi:10.1038/s41586-018-0532-1 Medline
30. J. Igea, A. J. Tanentzap, Angiosperm speciation cools down in the tropics. *Ecol. Lett.* **23**, 692–700 (2020). doi:10.1111/ele.13476 Medline
31. J. L. Brown, A. Cameron, A. D. Yoder, M. Vences, A necessarily complex model to explain the biogeography of the amphibians and reptiles of Madagascar. *Nat. Commun.* **5**, 5046 (2014). doi:10.1038/ncomms6046 Medline
32. B. J. Enquist, X. Feng, B. Boyle, B. Maitner, E. A. Newman, P. M. Jørgensen, P. R. Roehrdanz, B. M. Thiers, J. R. Burger, R. T. Corlett, T. L. P. Couvreur, G. Dauby, J. C. Donoghue, W. Foden, J. C. Lovett, P. A. Marquet, C. Merow, G. Midgley, N. Morueta-Holme, D. M. Neves, A. T. Oliveira-Filho, N. J. B. Kraft, D. S. Park, R. K. Peet, M. Pillet, J. M. Serra-Diaz, B. Sandel, M. Schildhauer, I. Šimová, C. Violle, J. J. Wieringa, S. K. Wiser, L. Hannah, J.-C. Svenning, B. J. McGill, The commonness of rarity: Global and future distribution of rarity across land plants. *Sci. Adv.* **5**, eaaz0414 (2019). doi:10.1126/sciadv.aaz0414 Medline

- 1001 33. P. W. Richards, Speciation in the tropical rain forest and the concept of the niche. *Biol. J.*
1002 *Linn. Soc.* **1**, 149–153 (1969). doi:10.1111/j.1095-8312.1969.tb01817.x
- 1003 34. J.-L. Mercier, L. Wilmé, The Eco-Geo-Clim model: Explaining Madagascar’s endemism.
1004 *Madag. Conserv. Dev.* **8**, 63–68 (2013). doi:10.4314/mcd.v8i2.3
- 1005 35. L. E. Lisiecki, M. E. Raymo, Plio–Pleistocene climate evolution: Trends and transitions in
1006 glacial cycle dynamics. *Quat. Sci. Rev.* **26**, 56–69 (2007). doi:10.1016/j.quascirev.2006.09.005
- 1007 36. J. S. Scheingross, A. B. Limaye, S. W. McCoy, A. C. Whittaker, The shaping of erosional
1008 landscapes by internal dynamics. *Nat. Rev. Earth Environ.* **1**, 661–676 (2020).
1009 doi:10.1038/s43017-020-0096-0
- 1010 37. T. Salles, P. Rey, E. Bertuzzo, Mapping landscape connectivity as a driver of species
1011 richness under tectonic and climatic forcing. *Earth Surf. Dyn.* **7**, 895–910 (2019).
1012 doi:10.5194/esurf-7-895-2019
- 1013 38. N. R. Gunawardene, A. E. Dulip Daniels, I. A. U. N. Gunatilleke, C. V. S. Gunatilleke, P. V.
1014 Karunakaran, K. Geetha Nayak, S. Prasad, P. Puyravaud, B. R. Ramesh, K. A. Subramanian, G.
1015 Vasanthi, A brief overview of the Western Ghats–Sri Lanka biodiversity hotspot. *Curr. Sci.* **93**,
1016 1567–1572 (2007).
- 1017 39. G. Murali, R. Gumbs, S. Meiri, U. Roll, Global determinants and conservation of
1018 evolutionary and geographic rarity in land vertebrates. *Sci. Adv.* **7**, eabe5582 (2021).
1019 doi:10.1126/sciadv.abe5582 Medline
- 1020 40. S. F. Gallen, Lithologic controls on landscape dynamics and aquatic species evolution in
1021 post-orogenic mountains. *Earth Planet. Sci. Lett.* **493**, 150–160 (2018).
1022 doi:10.1016/j.epsl.2018.04.029
- 1023 41. M. F. Stokes, D. Kim, S. F. Gallen, E. Benavides, B. P. Keck, J. Wood, S. L. Goldberg, I. J.
1024 Larsen, J. M. Mollish, J. W. Simmons, T. J. Near, J. T. Perron, Erosion of heterogeneous rock
1025 drives diversification of Appalachian fishes. *Science* **380**, 855–859 (2023).
1026 doi:10.1126/science.add9791 Medline
- 1027 42. A. J. Plumptre, T. R. B. Davenport, M. Behangana, R. Kityo, G. Eilu, P. Ssegawa, C.
1028 Ewango, D. Meirte, C. Kahindo, M. Herremans, J. K. Peterhans, J. D. Pilgrim, M. Wilson, M.
1029 Languy, D. Moyer, The biodiversity of the Albertine Rift. *Biol. Conserv.* **134**, 178–194 (2007).
1030 doi:10.1016/j.biocon.2006.08.021
- 1031 43. F. A. S. Cassemiro, J. S. Albert, A. Antonelli, A. Menegotto, R. O. Wüest, F. Cerezer, M. T.
1032 P. Coelho, R. E. Reis, M. Tan, V. Tagliacollo, D. Bailly, V. F. B. da Silva, A. Frota, W. J. da
1033 Graça, R. Ré, T. Ramos, A. G. Oliveira, M. S. Dias, R. K. Colwell, T. F. Rangel, C. H. Graham,
1034 Landscape dynamics and diversification of the megadiverse South American freshwater fish
1035 fauna. *Proc. Natl. Acad. Sci. U.S.A.* **120**, e2211974120 (2023). doi:10.1073/pnas.2211974120
1036 Medline
- 1037 44. G. Eagles, H. H. Hoang, Cretaceous to present kinematics of the Indian, African and
1038 Seychelles plates. *Geophys. J. Int.* **196**, 1–14 (2014). doi:10.1093/gji/ggt372

1039 45. L. Melluso, V. Morra, P. Brotzu, S. Tommasini, M. R. Renna, R. A. Duncan, L. Franciosi, F.
1040 D’Amelio, Geochronology and petrogenesis of the Cretaceous Antampombato–Ambatovy
1041 complex and associated dyke swarm, Madagascar. *J. Petrol.* **46**, 1963–1996 (2005).
1042 [doi:10.1093/petrology/egi044](https://doi.org/10.1093/petrology/egi044)

1043 46. J. M. Bardintzeff, J. P. Liégeois, B. Bonin, H. Bellon, G. Rasamimanana, Madagascar
1044 volcanic provinces linked to the Gondwana break-up: Geochemical and isotopic evidences for
1045 contrasting mantle sources. *Gondwana Res.* **18**, 295–314 (2010). [doi:10.1016/j.gr.2009.11.010](https://doi.org/10.1016/j.gr.2009.11.010)

1046 47. K. E. Samonds, I. S. Zalmout, M. T. Irwin, D. W. Krause, R. R. Rogers, L. L. Raharivony,
1047 *Eotheroides lambondrano*, new middle Eocene seacow (Mammalia, Sirenia) from the Mahajanga
1048 Basin, northwestern Madagascar. *J. Vertebr. Paleontol.* **29**, 1233–1243 (2009).
1049 [doi:10.1671/039.029.0417](https://doi.org/10.1671/039.029.0417)

1050 48. E. Laville, A. Piqué, J. C. Plaziat, P. Gioan, R. Rakotomalala, Y. Ravololonirina, E. Tidahy,
1051 Le fosse meridien d’Ankay-Alaotra, témoin d’une extension crustale récente et actuelle à
1052 Madagascar. *Bull. Soc. Géol. France* **169**, 775–788 (1998).

1053 49. J. Hackel, M. S. Vorontsova, O. P. Nanjarisoa, R. C. Hall, J. Razanatsoa, P. Malakasi, G.
1054 Besnard, Grass diversification in Madagascar: In situ radiation of two large C₃ shade clades and
1055 support for a Miocene to Pliocene origin of C₄ grassy biomes. *J. Biogeogr.* **45**, 750–761 (2018).
1056 [doi:10.1111/jbi.13147](https://doi.org/10.1111/jbi.13147)

1057 50. A. Gamisch, K. Winter, G. A. Fischer, H. P. Comes, Evolution of crassulacean acid
1058 metabolism (CAM) as an escape from ecological niche conservatism in Malagasy *Bulbophyllum*
1059 (Orchidaceae). *New Phytol.* **231**, 1236–1248 (2021). [doi:10.1111/nph.17437](https://doi.org/10.1111/nph.17437) [Medline](#)

1060 51. S. Federman, A. Dornburg, A. Downie, A. F. Richard, D. C. Daly, M. J. Donoghue, The
1061 biogeographic origin of a radiation of trees in Madagascar: Implications for the assembly of a
1062 tropical forest biome. *BMC Evol. Biol.* **15**, 216 (2015). [doi:10.1186/s12862-015-0483-1](https://doi.org/10.1186/s12862-015-0483-1) [Medline](#)

1063 52. C. G. Boluda, C. Christe, Y. Naciri, L. Gautier, A 638-gene phylogeny supports the
1064 recognition of twice as many species in the Malagasy endemic genus *Capurodendron*
1065 (Sapotaceae). *Taxon* **71**, 360–395 (2022). [doi:10.1002/tax.12676](https://doi.org/10.1002/tax.12676)

1066 53. D. J. Hearn, M. Evans, B. Wolf, M. McGinty, J. Wen, Dispersal is associated with
1067 morphological innovation, but not increased diversification, in *Cyphostemma* (Vitaceae). *J. Syst.*
1068 *Evol.* **56**, 340–359 (2018). [doi:10.1111/jse.12417](https://doi.org/10.1111/jse.12417)

1069 54. S. Faurby, W. L. Eiserhardt, W. J. Baker, J.-C. Svenning, An all-evidence species-level
1070 supertree for the palms (Arecaceae). *Mol. Phylogenet. Evol.* **100**, 57–69 (2016).
1071 [doi:10.1016/j.ympev.2016.03.002](https://doi.org/10.1016/j.ympev.2016.03.002) [Medline](#)

1072 55. D. N. Karger, O. Conrad, J. Böhner, T. Kawohl, H. Kreft, R. W. Soria-Auza, N. E.
1073 Zimmermann, H. P. Linder, M. Kessler, Climatologies at high resolution for the earth’s land
1074 surface areas. *Sci. Data* **4**, 170122 (2017). [doi:10.1038/sdata.2017.122](https://doi.org/10.1038/sdata.2017.122) [Medline](#)

1075 56. Y. Wang, yanyanwangesd/DAC-weaksurfacelayer: DAC-Escarpment-weaksurfacelayer,
1076 version 1.0.0, Zenodo (2023); <https://doi.org/10.5281/zenodo.7686096>.

1077 57. Y. Wang, yanyanwangesd/landscape_physiographic_patchness: Initial release, version 1.0.0,
1078 Zenodo (2023); <https://doi.org/10.5281/zenodo.8302036>.

1079 58. Y. Liu, Y. Wang, S. Willett, N. E. Zimmermann, L. Pellissier, Escarpment evolution drives
1080 the diversification of the Madagascar flora, EnviDat (2023);
1081 <https://www.doi.org/10.16904/enviDat.387>.

1082 59. M. Ohba, K. E. Samonds, M. LaFleur, J. R. Ali, L. R. Godfrey, Madagascar's climate at the
1083 K/P boundary and its impact on the island's biotic suite. *Palaeogeogr. Palaeoclimatol.*
1084 *Palaeoecol.* **441**, 688–695 (2016). doi:10.1016/j.palaeo.2015.10.028

1085 60. H. E. Beck, N. E. Zimmermann, T. R. McVicar, N. Vergopolan, A. Berg, E. F. Wood,
1086 Present and future Köppen-Geiger climate classification maps at 1-km resolution. *Sci. Data* **5**,
1087 180214 (2018). doi:10.1038/sdata.2018.214 Medline

1088 61. D. R. Davies, A. P. Valentine, S. C. Kramer, N. Rawlinson, M. J. Hoggard, C. M. Eakin, C.
1089 R. Wilson, Earth's multi-scale topographic response to global mantle flow. *Nat. Geosci.* **12**, 845–
1090 850 (2019). doi:10.1038/s41561-019-0441-4

1091 62. L. Brosens, R. Cox, B. Campforts, L. Jacobs, V. Vanacker, P. Bierman, V. F.
1092 Razanamahandry, A. F. M. Rakotondrazafy, T. Razafimbelo, T. Rafolisy, G. Govers, The slow
1093 downwearing of Madagascar: Inferring patterns and controls on long-term basin-averaged
1094 erosion rates from *in situ* ¹⁰Be at the catchment and regional level. *Earth Surf. Process. Landf.*
1095 **48**, 1765–1782 (2023). doi:10.1002/esp.5586

1096 63. J.-Y. Roig, R. D. Tucker, S. G. Peters, C. Delor, H. Theveniaut, *Carte Géologique de la*
1097 *République de Madagascar à 1/1,000,000* (Ministère des Mines, Géologie Programme de
1098 Gouvernance des Ressources Minérales, 2012).

1099 64. H. Morlon, Phylogenetic approaches for studying diversification. *Ecol. Lett.* **17**, 508–525
1100 (2014). doi:10.1111/ele.12251 Medline

1101 65. H. Morlon, E. Lewitus, F. L. Condamine, M. Manceau, J. Clavel, J. Drury, RPANDA: An R
1102 package for macroevolutionary analyses on phylogenetic trees. *Methods Ecol. Evol.* **7**, 589–597
1103 (2016). doi:10.1111/2041-210X.12526

1104 66. D. Burnham, K. Anderson, *Model Selection and Inference: A Practical Information-*
1105 *Theoretic Approach* (Springer, 2002).

1106 67. Y. Jin, H. Qian, V. PhyloMaker: An R package that can generate very large phylogenies for
1107 vascular plants. *Ecography* **42**, 1353–1359 (2019). doi:10.1111/ecog.04434

1108 68. A. Guisan, N. E. Zimmermann, Predictive habitat distribution models in ecology. *Ecol.*
1109 *Modell.* **135**, 147–186 (2000). doi:10.1016/S0304-3800(00)00354-9

1110 69. Missouri Botanical Garden, Tropicos, v3.2.3 (2021); <https://tropicos.org>.

1111 70. GBIF.org, GBIF Occurrence Download (2021); <https://doi.org/10.15468/dl.66u4gm>.

1112 71. B. J. Enquist, R. Condit, R. K. Peet, M. Schildhauer, B. M. Thiers, Cyberinfrastructure for an
 1113 integrated botanical information network to investigate the ecological impacts of global climate
 1114 change on plant biodiversity. *PeerJ Prepr.* **4**, e2615v2 (2016).
 1115 [doi:10.7287/peerj.preprints.2615v2](https://doi.org/10.7287/peerj.preprints.2615v2)

1116 72. L. M. Page, B. J. MacFadden, J. A. Fortes, P. S. Soltis, G. Riccardi, Digitization of
 1117 biodiversity collections reveals biggest data on biodiversity. *Bioscience* **65**, 841–842 (2015).
 1118 [doi:10.1093/biosci/biv104](https://doi.org/10.1093/biosci/biv104)

1119 73. G. Dauby, R. Zaiss, A. Blach-Overgaard, L. Catarino, T. Damen, V. Deblauwe, S. Dessein, J.
 1120 Dransfield, V. Droissart, M. C. Duarte, H. Engledow, G. Fadeur, R. Figueira, R. E. Gereau, O. J.
 1121 Hardy, D. J. Harris, J. de Heij, S. Janssens, Y. Klomberg, A. C. Ley, B. A. Mackinder, P. Meerts,
 1122 J. L. van de Poel, B. Sonké, M. S. Sosef, T. Stévant, P. Stoffelen, J. C. Svenning, P. Sepulchre,
 1123 X. van der Burgt, J. J. Wieringa, T. L. Couvreur, RAINBIO: A mega-database of tropical
 1124 African vascular plants distributions. *PhytoKeys* **74**, 1–18 (2016).
 1125 [doi:10.3897/phytokeys.74.9723](https://doi.org/10.3897/phytokeys.74.9723) Medline

1126 74. S. Chamberlain, D. Oldoni, L. Geffert, P. Desmet, V. Barve, K. Ram, D. McGlinn, J. Ooms,
 1127 S. S. Ye, J. Oksanen, B. Marwick, J. Baumgartner, M. Sumner, Sriram, ropensci/rgbif: rgbif
 1128 v3.3.0, version 3.3.0, Zenodo (2020); <https://doi.org/10.5281/zenodo.4019238>.

1129 75. A. Zizka, D. Silvestro, T. Andermann, J. Azevedo, C. Duarte Ritter, D. Edler, H. Farooq, A.
 1130 Herdean, M. Ariza, R. Scharn, S. Svantesson, N. Wengström, V. Zizka, A. Antonelli,
 1131 CoordinateCleaner: Standardized cleaning of occurrence records from biological collection
 1132 databases. *Methods Ecol. Evol.* **10**, 744–751 (2019). [doi:10.1111/2041-210X.13152](https://doi.org/10.1111/2041-210X.13152)

1133 76. T. Hengl, J. Mendes de Jesus, G. B. M. Heuvelink, M. Ruiperez Gonzalez, M. Kilibarda, A.
 1134 Blagotić, W. Shangguan, M. N. Wright, X. Geng, B. Bauer-Marschallinger, M. A. Guevara, R.
 1135 Vargas, R. A. MacMillan, N. H. Batjes, J. G. B. Leenaars, E. Ribeiro, I. Wheeler, S. Mantel, B.
 1136 Kempen, SoilGrids250m: Global gridded soil information based on machine learning. *PLOS*
 1137 *ONE* **12**, e0169748 (2017). [doi:10.1371/journal.pone.0169748](https://doi.org/10.1371/journal.pone.0169748) Medline

1138 77. L. Lyu, F. Leugger, O. Hagen, F. Fopp, L. M. Boschman, J. S. Strijk, C. Albouy, D. N.
 1139 Karger, P. Brun, Z. Wang, N. E. Zimmermann, L. Pellissier, An integrated high- resolution
 1140 mapping shows congruent biodiversity patterns of *Fagales* and *Pinales*. *New Phytol.* **235**, 759–
 1141 772 (2022). [doi:10.1111/nph.18158](https://doi.org/10.1111/nph.18158) Medline

1142 78. J. A. Nelder, R. W. Wedderburn, Generalized linear models. *J. R. Stat. Soc. Ser. A* **135**, 370–
 1143 384 (1972). [doi:10.2307/2344614](https://doi.org/10.2307/2344614)

1144 79. T. Hastie, R. Tibshirani, Exploring the nature of covariate effects in the proportional hazards
 1145 model. *Biometrics* **46**, 1005–1016 (1990). [doi:10.2307/2532444](https://doi.org/10.2307/2532444) Medline

1146 80. J. H. Friedman, Greedy function approximation: A gradient boosting machine. *Ann. Stat.* **29**,
 1147 1189–1232 (2001). [doi:10.1214/aos/1013203451](https://doi.org/10.1214/aos/1013203451)

1148 81. L. Breiman, Random forests. *Mach. Learn.* **45**, 5–32 (2001). [doi:10.1023/A:1010933404324](https://doi.org/10.1023/A:1010933404324)

1149 82. P. Brun, W. Thuiller, Y. Chauvier, L. Pellissier, R. O. Wüest, Z. Wang, N. E. Zimmermann,
1150 Model complexity affects species distribution projections under climate change. *J. Biogeogr.* **47**,
1151 130–142 (2020). doi:10.1111/jbi.13734

1152 83. O. Allouche, A. Tsoar, R. Kadmon, Assessing the accuracy of species distribution models:
1153 Prevalence, kappa and the true skill statistic (TSS). *J. Appl. Ecol.* **43**, 1223– 1232 (2006).
1154 doi:10.1111/j.1365-2664.2006.01214.x

1155 84. A. Jarvis, H. I. Reuter, A. Nelson, E. Guevara, Hole-filled SRTM for the globe, version 4
1156 (2008); <https://srtm.csi.cgiar.org/>.

1157 85. J. Moat, P. Smith, *Atlas de La Vegetation de Madagascar* (Royal Botanic Gardens, 2007).

1158 86. The Nature Conservancy, “Terrestrial Ecosystems: Global Ecoregions, Major Habitat Types,
1159 Biogeographical Realms and The Nature Conservancy Terrestrial Assessment Units as of
1160 December 14, 2009” (2009);
1161 <https://geospatial.tnc.org/datasets/b1636d640ede4d6ca8f5e369f2dc368b/about>.

1162 87. S. W. Laffan, M. D. Crisp, Assessing endemism at multiple spatial scales, with an example
1163 from the Australian vascular flora. *J. Biogeogr.* **30**, 511–520 (2003). doi:10.1046/j.1365-
1164 2699.2003.00875.x

1165 88. S. Dray, A.-B. Dufour, The ade4 package: Implementing the duality diagram for ecologists.
1166 *J. Stat. Softw.* **22**, 1–20 (2007). doi:10.18637/jss.v022.i04

1167 89. K. X. Whipple, G. E. Tucker, Dynamics of the stream-power river incision model:
1168 Implications for height limits of mountain ranges, landscape response timescales, and research
1169 needs. *J. Geophys. Res.* **104**, 17661–17674 (1999). doi:10.1029/1999JB900120

1170 90. R. Punchi-Manage, S. Getzin, T. Wiegand, R. Kanagaraj, C. V. Savitri Gunatilleke, I. A. U.
1171 Nimal Gunatilleke, K. Wiegand, A. Huth, Effects of topography on structuring local species
1172 assemblages in a Sri Lankan mixed dipterocarp forest. *J. Ecol.* **101**, 149– 160 (2013).
1173 doi:10.1111/1365-2745.12017

1174 91. Z. Wang, W. Ye, H. Cao, Z. Huang, J. Lian, L. Li, S. Wei, I.-F. Sun, Species–topography
1175 association in a species-rich subtropical forest of China. *Basic Appl. Ecol.* **10**, 648– 655 (2009).
1176 doi:10.1016/j.baae.2009.03.002

1177

1178 92. G. G. Simpson, Mammals and the nature of continents. *Am. J. Sci.* **241**, 1–31 (1943).
1179 doi:10.2475/ajs.241.1.1

1180 93. J. J. Lennon, P. Koleff, J. Greenwood, K. J. Gaston, The geographical structure of British
1181 bird distributions: Diversity, spatial turnover and scale. *J. Anim. Ecol.* **70**, 966–979 (2001).
1182 doi:10.1046/j.0021-8790.2001.00563.x

1183 94. C. H. Graham, P. V. Fine, Phylogenetic beta diversity: Linking ecological and evolutionary
1184 processes across space in time. *Ecol. Lett.* **11**, 1265–1277 (2008). doi:10.1111/j.1461-
1185 0248.2008.01256.x Medline

- 1186 95. S. W. Laffan, D. F. Rosauer, G. Di Virgilio, J. T. Miller, C. E. González-Orozco, N. Knerr,
1187 A. H. Thornhill, B. D. Mishler, Range-weighted metrics of species and phylogenetic turnover
1188 can better resolve biogeographic transition zones. *Methods Ecol. Evol.* **7**, 580–588 (2016).
1189 [doi:10.1111/2041-210X.12513](https://doi.org/10.1111/2041-210X.12513)
- 1190 96. B. H. Daru, M. van der Bank, O. Maurin, K. Yessoufou, H. Schaefer, J. A. Slingsby, T. J.
1191 Davies, A novel phylogenetic regionalization of phytogeographical zones of southern Africa
1192 reveals their hidden evolutionary affinities. *J. Biogeogr.* **43**, 155–166 (2016).
1193 [doi:10.1111/jbi.12619](https://doi.org/10.1111/jbi.12619)
- 1194 97. R. R. Sokal, F. J. Rohlf, The comparison of dendrograms by objective methods. *Taxon* **11**,
1195 33–40 (1962). [doi:10.2307/1217208](https://doi.org/10.2307/1217208)
- 1196 98. B. H. Daru, P. Karunaratne, K. Schliep, phyloregion: R package for biogeographical
1197 regionalization and macroecology. *Methods Ecol. Evol.* **11**, 1483–1491 (2020).
1198 [doi:10.1111/2041-210X.13478](https://doi.org/10.1111/2041-210X.13478)
- 1199 99. P. Brun, N. E. Zimmermann, C. Hari, L. Pellissier, D. N. Karger, Global climate-related
1200 predictors at kilometer resolution for the past and future. *Earth Syst. Sci. Data* **14**, 5573–5603
1201 (2022). [doi:10.5194/essd-14-5573-2022](https://doi.org/10.5194/essd-14-5573-2022)
- 1202 100. A. Liaw, randomForest: Breiman and Cutler’s Random Forests for Classification and
1203 Regression, R package version 4.7-1 (2022); [https://CRAN.R-](https://CRAN.R-project.org/package=randomForest)
1204 [project.org/package=randomForest](https://CRAN.R-project.org/package=randomForest).
- 1205 101. J. Tan, G. J. Huffman, D. T. Bolvin, E. J. Nelkin, IMERG V06: Changes to the morphing
1206 algorithm. *J. Atmos. Ocean. Technol.* **36**, 2471–2482 (2019). [doi:10.1175/JTECH-D-19-0114.1](https://doi.org/10.1175/JTECH-D-19-0114.1)